Faculty of Science

Thermal properties in different rock materials based on Hot Disk and mineral mode - a comparison between petrographic analysis and laboratory measurements

Emil Andersson

Degree of Master of Science (120 credits)
with a major in Earth Sciences
30 hec

Department of Earth Sciences
University of Gothenburg
2016 B907

UNIVERSITY OF GOTHENBURG

UNIVERSITY OF GOTHENBURG
Department of Earth Sciences
Geovetarcentrum/Earth Science Centre

Thermal properties in different rock materials based on Hot Disk and mineral mode - a comparison between petrographic analysis and laboratory measurements

Emil Andersson

ISSN 1400-3821

B907
Master of Science (120 credits) thesis
Göteborg 2016

Mailing address	**Address**	**Telephone**	**Telefax**	
Geovetarcentrum S 405 30 Göteborg	Geovetarcentrum Guldhedsgatan 5A	031-786 19 56	031-786 19 86	Geovetarcentrum Göteborg University S-405 30 Göteborg SWEDEN

Abstract

Keywords: *Thermal conductivity, heat capacity, Hot Disk TPS, petrography, mineral mode*

The different thermal properties of rock material are being more frequently applied to industry and infrastructural projects where knowledge about thermal conductivity and heat capacity is especially sought after. This study has examined thermal conductivity and heat capacity of different rock types using the Hot Disk TPS (Transient Plane Source) method and compared these results to tabulated literature values of the constituting minerals and their relative proportions, in order to determine whether the latter could suffice as an alternative method and if certain petrographic parameters (mineralogy, grain size and microstructure) affect this method. Rock samples were cut into specimens, which were measured with the TPS method, and thin-section material, which was analyzed for petrographic parameters. The results showed that thermal conductivity correlated strongly with mineral content (especially quartz) in the specimens, whereas heat capacity showed no clear connection from mafic to felsic mineralogy. The investigated petrographic parameters may have contributed to a decrease in thermal conductivity but most likely not in heat capacity. The study showed that the calculated thermal conductivity values correlated moderately (R^2= 0.44) to strongly (R^2= 0.88). It was concluded that the method may function as an economical and environmental alternative to the TPS-method but should be used with caution due to the presented limitations.

Sammanfattning

Nyckelord: *Termisk ledningsförmåga, värmekapacitet, Hot Disk TPS, petrografi, mineralinnehåll*

Termiska egenskaper i bergsprodukter tillämpas numera allt oftare inom industri och infrastruktur där kunskap om termisk ledningsförmåga och värmekapacitet är väldigt eftersökta. Denna studie har undersökt termisk ledningsförmåga och värmekapacitet genom att jämföra Hot Disk TPS mätningar av ett antal bergarter med listade litteraturvärden för ingående mineral och dess andel, för att undersöka om detta räcker som ett alternativ till det förstnämnda, där även olika petrografiska parametrars inverkan undersöktes (mineralogi, kornstorlek samt mikrostruktur). Stenprover samlades in och sågades till som provkroppar för TPS metoden och tunnslip för petrografisk analys. Studien visade att mineralogi korrelerar (speciellt kvartsinnehåll) med ledningsförmågan, men inte lika tydligt för värmekapacitet. De undersökta petrografiska parametrarna kan ha bidragit till en minskning i ledningsförmåga men förmodligen inte i värmekapacitet. Studien visar även att den uppmätta och beräknade ledningsförmågan korrelerade måttligt (R^2=0.44) till starkt (R^2=0.88). Det sammanfattades att metoden kan fungera som ett ekonomiskt och miljömässigt alternativ, men måste då användas med försiktighet p.g.a. de presenterade begränsningarna.

Contents

1. Introduction

Rock material (as aggregate, dimension stone or bedrock) is more frequently being utilized in complex industrial and infrastructural applications where specific knowledge about thermal properties is required. High-quality rock materials with the ability to conduct, insulate or store thermal energy are therefore requested in projects due to certain technical applications and the increasing environmental awareness of energy saving. Technical applications include heat transport away from high-voltage ground cables to avoid thermal failure of the cable, safe dimensioning of nuclear waste storage in bedrock and use of dimension stone facade elements with respect to fire regulations.

Thermal conductivity in crystalline bedrock is an especially important property which has been investigated in several research projects. Different petrographic parameters have therefore been reviewed, where the correlation between mineral content and thermal conductivity is deemed to be the most relevant parameter (Sundberg et al., 1985; Sundberg et al., 2009). Other important parameters related to thermal properties are the structure, density, porosity, texture, micro-cracks and moisture content of the material (Clauser & Huenges, 1995). In research conducted by Swedish Cement and Concrete Research Institute (CBI) together with Lund University (Herlin, 2014, Chan, 2013), measurements of thermal properties were performed on concrete made up of different aggregate. They concluded that thermal conductivity of aggregates was reflected in the resulting concrete and that high thermal conductivity gave higher thermal shock resistance. This thesis will partly build on Chan's previous work (2013) by using some rock types from the same quarry but instead focus on the mineralogical perspective of thermal conductivity and heat capacity.

Thermal properties in crystalline materials have traditionally been approached with direct laboratory instruments, where the measured response of temperature over time has been used to calculate thermal conductivity, heat capacity and thermal diffusivity in a material. This type of method yields valid data about thermal properties but is costly and time consuming due to the sample preparation and conditioning, where also the availability of good material in the right dimension (core drilling projects) may be limiting. Birch & Clark, (1940), Clark (1966), Horai & Simmons, (1969), Horai, (1971) and Baldridge & Horai (1972) proposed that thermal conductivity and heat capacity could theoretically be calculated for crystalline rocks without the use of laboratory instruments. The authors thereby measured and listed values for thermal conductivity of over 100 individual mineral phases that could be utilized to theoretically calculate the thermal conductivity of a rock, using only petrographic analysis of modal composition. Petrographic analysis together with point counting is a relatively quick and cheap method in contrast to laboratory measurements to gain information about modal composition. This self-estimate approach has been confirmed by previously mentioned authors to yield reasonable data (Baldridge & Horai, 1972) for thermal properties compared to direct measurements, where mineral mode is claimed to correlate with thermal conductivity. However, other studies have

shown that thermal conductivity does not necessarily have to be in good correlation with mineralogical composition and may fluctuate greatly from location to location and rock type to rock type (Andolfsson, 2013).

This work will compare thermal properties from selected block-size rock specimens of varying modal composition, obtained with the Hot Disk - Transient Plane Source (TPS) instrument against thermal data from literature and mineral mode (optical microscopy) as an attempt to evaluate if thermal properties can be predicted without laboratory instruments. If the method is successful, this will allow a more beneficial way to save time and money, as well as reduce the use of energy resources in future projects. This could then be applied to industry by more efficiently investigating thermal properties of different types of rock materials such as dimension stone, larger blocks, aggregates and land beds. The correlated relationship between petrography and thermal properties may later be used in extensive modeling and statistical analyses.

1.1 Research questions

How well does thermal conductivity and heat capacity actually correlate with mineral content in crystalline rock types and how do they differ?

Is the correlation sufficient to use petrographic analysis (i.e. mineral mode) and tabulated mineral values as a basis for estimating thermal conductivity and heat capacity, instead of laboratory measurement procedures? Can this methodology be of economic and environmental interest when investigating thermal properties of rock materials in the future?

How do microstructure and mineral grain-size affect thermal conductivity and heat capacity in the crystalline rock?

1.2 Limitations

Initially stated, this report will only address certain concepts and laws of thermodynamics as it otherwise will result in complexity beyond the extent of this project. The project will focus solely on aspects related to mineralogy and petrography as it is the aim of the project, but will however provide a general background on the matter in order for the reader to understand relevant concepts of the study.

2. Background to thermal properties in rocks and their applications

Thermal properties in rocks have a variety of applications in industry, infrastructure and even nuclear waste storage, where it is considered very important. There are several European product standards for declaring thermal conductivity (EN 1469, 12057 and 12058) of rock material used for dimension stone in architectural purposes. Rock material with high thermal conductivity is requested in projects by e.g. Svenska Kraftnät (Swedish electricity operator), where large electrical cables are put into land beds of aggregates with quartz content of at least 30 % (but in some critical cases 85 % is demanded). This requirement is demanded to reduce accidents of heat development in cases of unforeseen thermic collapse in the cables, where the land beds with high

quartz content will serve as medium of conduction (Sundberg, 1991). Conduction of heat in crystalline bedrock is especially important for use of geothermal energy and geothermal wells, which is regarded as a promising renewable alternative to traditional energy sources (Sundberg, 1991). In other applications, there is instead a demand for rock material or clays which have low conductive abilities. One example is for energy or infrastructural purposes where the surrounding bedrock or bearing stratum is demanded to have low conductivity to minimize the loss of thermal energy in long-distance heating pipes or heating culverts (Sundberg, SGI, 1991). Heat properties in concrete have been studied to se if large scale energy losses inside buildnings could be prevented, where the thermal properties of the aggregates used in the concrete reflect the ability to store heat (Chan, 2013, Herlin 2014). Thermal properties in crystalline bedrock have been thoroughly investigated by SKB (Swedish Nuclear Fuel and Waste Management Company) to ensure that the storage space for nuclear waste meets the strict requirements and to prospect for new sites of long-term waste storage canisters (Sundberg et al., 2008).

3. Geology and background information of sampled aggregates

3.1 Forserum - quartzite and diabase

Skanska has operated a quartzite and diabase quarry since the early forties in the area of Forserum close to Jönköping. The geology of the quarry in Forserum belongs to the Almesåkra-formation, which is characterized by thick sedimentary sequences of red to white feldsphatic sandstones, shales and conglomerates together with banded quartzites. The sequence has been interpreted as Jotnian flood deposits which in turn overly the magmatic rocks in the Oskarshamn – Jönköpingbelt (OJB), (Lundqvist et al., 2011). The sedimentary bedrock displays disconformities and faulting from the erosion and tectonic movement of the Sveconorwegian orogeny (Lundqvist et al., 2011). The Almesåkra formation and adjacent older bedrock (OJB and the Transscandinavian Igenous Belt, TIB) are cut by several N-S trending diabase dykes belonging to the Blekinge-Dalarna Dolorites (BDD), dated to 954 ± 1.2 Ma by U-Pb baddeleyite (Söderlund et al., 2004). The diabase and quartzite at the Forserum location is used for infrastructural purposes in asphalt and in railway constructions due to their durability (mainly abrasion resistance).

3.2 Gillstad – gabbro

This quarry is owned and managed by Swerock AB and is located in Gillstad near Lidköping. The material is situated in one of several tectonic lenses within the Mylonite zone where the composition of the body is mafic to ultramafic. The main rock types range from gabbro to diorite, but can occur as a metamorphosed medium grained and weakly foliated amphibolite. An ultramafic body 20 km SSW of the Gillstad quarry has previously been studied and dated by the Re-Os method, yielding an age of 1887 Ma (Scherstén, 2002), in sharp contrast to the 1700 Ma Eastern Segment and 1600 Ma Idefjorden Terrane rocks, directly to the east and west, respectively, of the Mylonite zone. Gabbro generally has varied usages but is commonly used

within the construction industry and as railway aggregate. If obtained in good quality, it may also be used for architectural purposes, such as exterior facing stone, panels and floor tiles.

3.3 Flivik - granite

This granite is quarried in Figeholm (Flivik quarry) between the cities of Västervik and Oskarshamn, where it has been mined since the early 20th century to produce dimension stone and crushed aggregates. The quarry is currently owned by Emmaboda Granit AB, which today produce dimension stone for house interior and house facade purposes. The Flivik granite is a red Småland-värmland granite with a gray-lilac tint and varying grain size, which is part of the 1810-1760 Ma TIB-1generation (Lundqvist et al., 2011). The Småland granitoids are often associated with the Småland porphyries which have similar ages and geochemistry but are of volcanic origin.

3.4 Fröland - granite with pegmatite

The Fröland quarry is located in the town of Uddevalla on the Swedish west coast and is currently owned and managed by Swerock. Uddevalla has been part of the important stone cutting business since the mid-19th century which historically has provided stone material for ornament stones, building stones and road material, nationally and internationally. The material produced in Fröland is associated with the Bohus granite, with pegmatite dikes as a common feature in the quarry. Fröland is geologically positioned in the Idefjorden Terrane, where the Bohus granite intruded 920 Ma (Eliasson & Schöberg, 1991), coeval with e.g. the Blomskog granite in SW Värmland. The magma generating the Bohus granite intrusion is probably late to post-collision in relation to the Sveconorwegian orogeny, with Stora Le Marstrand (SLM) formation as a likely source (Eliasson & Schöberg, 1991).

3.5 Bårarp – granitic gneiss

The Bårarp quarry is located in Getinge between the cities of Falkenberg and Halmstad and has been quarried by Emmaboda Granit AB since the seventies. The Bårarp gneiss (or rather migmatite) is mostly used for dimension stone and construction stone purposes. The rock type found in Bårarp is often referred to as “Hallandia gneiss” after the region where it is quarried. Geologically, the Bårarp migmatite is part of the Eastern Segment of the Sveconorwegian Province, is mostly fine- to medium grained with a strongly foliated fabric where both amphibole and biotite are present and is irregularly and diffusely veined. The Bårarp migmatite is the product of two events of regional metamorphism and deformation, the 1460-1380 Ma Hallandian orogeny and the 970 Ma Sveconorwegian orogeny (Möller et al,. 2007).

4. Heat and thermal properties

4.1 Thermal energy and heat

Energy can occur in different forms, e.g., electrical, thermal, mechanical and chemical, which can be exchanged with another but not be destroyed or created (Best, 2003). Chemical internal energy

in a matter can be kinetic or potential, where the former involves the energy stored in molecular movements through translation, rotation and vibration, and the latter with the intermolecular forces (Best, 2003). In thermodynamics, the concept of kinetic and potential energy (movement and positing of atoms, respectively) can be referred to as thermal energy, which manifests itself as the temperature of a system (Best, 2003). An increase in molecular movement in a matter increases the thermal energy in the matter, which in turn will increase the temperature (Best, 2003). An increase in temperature of a system will generate a thermal energy gradient which according to the laws of thermodynamics will cause energy to move from a high to low state (Best, 2003). Thermal energy itself can be seen as a property of a thermodynamic system and may occur both within and outside the system boundary (Best, 2003). A thermodynamic system (Figure 1) is a part of our universe with specified or unspecified properties (Faure, 1998) and can be open, closed, isolated or adiabatic. This section will very briefly describe open and closed system as they are relevant to the report. The open system is very common in geology and is a state where both matter and energy can flow freely through the boundary of the system. In the closed system, energy may flow through the system boundary freely but the mass will remain constant (Best, 2003).

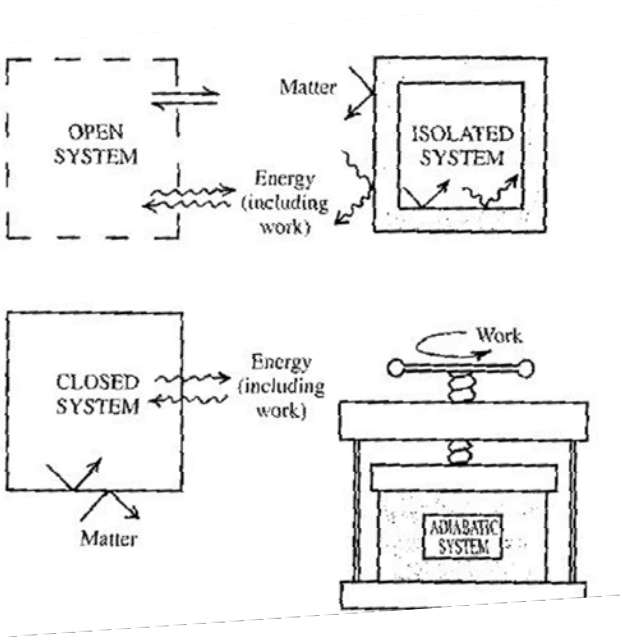

Figure 1. The different systems in thermodynamics and their relation to mass, energy and work (Best, 2003).

Heat is easy to confuse with thermal energy but is actually the transfer of thermal energy within a system or across a thermodynamic system boundary generated by a temperature difference (hot to cold). The sign of the heat quantity depend on the direction: into the system is positive due to addition of heat, out of the system is negative due to loss of heat. Work is also a part of thermodynamic systems and is caused by changes of pressure and/or volume, and is a separate

quantity which also can be positive or negative (Faure, 1998). The most important heat transfer (heat flow) mechanisms in nature are conduction, convection, advection and radiation, where conduction is the most important for rocks and aggregates as these are solids. Heat flow can be seen as the temperature gradient multiplied with the thermal conductivity (Equation 1). Heat is also related to other thermal properties such as specific heat capacity (the ability of a material to store heat) and thermal diffusivity (how fast heat is conducted through a surface of a material).

4.2 Heat in a geological perspective

Heat flow or movement of thermal energy is the fundamental driving process within the earth, responsible for forming and reforming solid rock through melts and tectonic plate movements. There are commonly four ways that thermal heat is transferred: conduction, convection, advection and radiation (Best, 2003). Conduction is the transfer of vibrations (kinetic energy of atoms) within a material, whereas convection is the movement of the material itself (gas, liquid or ductile rock) due to density difference caused by temperature difference or compositional variations (Best, 2003). In advection, a fluid phase of different temperature flows through the openings of a colder solid matter. Radiation on the other hand is a phenomenon where energy is emitted as electromagnetic waves due to spontaneous changes in electronic configurations in atoms or molecules (Best, 2003). However, compared to conduction, radiation is not very important in solid opaque rocks.

4.3 Thermal conductivity

Thermal conductivity was briefly described in the sections above and is the ability to transport thermal energy trough a material. Thermal conductivity can be seen as the ability of material to conduct heat and is related to rocks and minerals by the movements of free electrons and/or the vibrations of stationary atoms, ions or molecules through a lattice (Çengel & Boles, 2006). The arrangement of atoms in the lattice is therefore an important aspect for crystalline materials' conductive ability as it generates the vibrational framework (Birch & Clark, 1940). Metals on the other hand are more influenced by the electrical component (i.e. movement paths of electrons). Rock material is generally considered to have low thermal conductivity compared to some metals and ceramic products, and can instead be considered as insulators (Best, 2003). Some crystalline materials, such as diamond, have extremely high thermal conductivity due to its highly ordered structure (Table 1). Thermal conductivity can be described using Fourier´s law (Çengel & Boles, 2006).

$$q = -\lambda \frac{dT}{dx} \qquad (1)$$

Here q is the heat flow over an area (W/m^2), λ is the thermal conductivity (W/mK), T is the temperature difference in K (Kelvin) and x is the thickness of a layer (sometimes regarded as distance). The equation demonstrates that heat is conducted in the same direction as the temperature gradient ($\frac{dT}{dx}$) vector, where the equation is modified from the initial equation with a negative sign to allow heat transfer to be positive from higher to lower temperature (Çengel &

Boles, 2006). Due to the included time factor in the heat flow (i.e. W=J/s), the equation holds no further time factor.

The heat flow in rocks or other polycrystalline material is often limited by a resistance of the heat flow between interfaces (grain boundaries) of the different mineral grains, which will cause vibrations to scatter at the interface. This thermal resistance is called thermal boundary resistance or the Kapitza resistance.

$$q = -\frac{\Delta T}{\mathrm{R}} \qquad (2)$$

q is still heat flow, ΔT is still temperature difference and R is the heat transfer resistance (W/m^2K) (Çengel & Boles, 2006).

Table 1. Demonstration of thermal conductivities at normal room condition for different materials (modified after Çengel & Boles, 2006).

Material	**Thermal conductivity (W/m K)**
Diamond	2300
Silver	429
Copper	401
Gold	317
Aluminum	237
Iron	80.2
Glass	1.4

4.4 Heat capacity

When thermal conductivity represents the property to transport thermal energy throughout a material, heat capacity or thermal capacity is the capability to store heat as energy inside a material or substance. Heat capacity can have a variety of names in literature such as heat capacity, specific heat capacity, molar heat capacity or volumetric heat capacity with slightly different meaning related to unit of the substance: mass, mole or volume (Çengel & Boles, 2006). Specific heat capacity can be described as the resulting change of the temperature inside a material or substance by one Kelvin or degree due to the addition of heat. This process requires different amounts of energy depending on material (Çengel & Boles, 2006). Crystalline minerals and rocks are more accurately described by either specific or volumetric capacity as they refer to energy being transferred and stored inside the materials (Çengel & Boles, 2006). Equation 3 and 4 show the relationship between specific heat capacity and volumetric heat capacity:

$$C_v = \frac{Q}{V\Delta T} \qquad (3)$$

$$C_v = \rho * C_p \qquad (4)$$

In Equation 3, C_v represents the volumetric heat capacity (J/m^{3}K), Q the heat input (J), V the volume, (m^3) and ΔT the change in temperature (K). Equation 4 defines volumetric heat capacity as the specific heat C_p (J/kg K) multiplied with density ρ (kg/m^3). C_p can be applied to mineral components in rocks when multiplied with the known volume fraction in a sample (Schön, 2011).

4.5 Thermal diffusivity

Thermal diffusivity is a term which also should be mentioned in this section as it describes the relation between thermal conductivity and volumetric heat capacity (Çengel & Boles, 2006). Thermal diffusivity can be explained as how fast heat is transported in material. The following equation describes thermal diffusivity:

$$\alpha = \frac{\lambda}{C_V} \tag{5}$$

α is thermal diffusivity (m^2/s), C_V is the volumetric heat capacity (J/m^{3}K) and λ is the thermal conductivity (W/mK).

4.6 Thermal properties of rocks and rock forming minerals

Thermal properties of rocks and minerals have been measured and analyzed extensively throughout the 20th century by several researchers (Birch & Clark, 1940, Clark, 1966, Horai & Simmons, 1969, Horai, 1970, Hashin & Shtrikman, 1962 and Clauser & Huenges, 1995). Since then, other authors have continued to explain the petrographic factors and parameters related to thermal properties in rocks and minerals. Most authors strongly argue that mineralogy is the most important factor for thermal properties in igneous and metamorphic rocks and in some instances also in sedimentary rocks. The density of crystalline rock and minerals are also argued to have a clear relation to thermal properties, where a closely arranged structure inside a material lowers the resistance of heat transfer from one point to another (Sundberg et al., 2009). The majority of studies on thermal conductivity have however been carried out on sedimentary rocks due to the oil and gas industry. Thermal conductivity in sedimentary rocks are affected by slightly different parameters than igneous rocks where porosity, moist content and diagenetic factors (layering etc.) contribute to conductive abilities (Clauser & Huenges, 1995). The various processes of producing sedimentary, igneous and metamorphic rocks will ultimately contribute to different controlling factors in thermal conductivity in any given rock, where slight variations may occur in a specific rock type from location to location.

4.6.1 Porosity

Thermal conductivity of sedimentary and extrusive volcanic rocks is mostly controlled by the degree of porosity and saturation of pores compared to igneous rock types with low porosity (Clauser & Huenges, 1995). Porosity can occur both due to sedimentary processes as well as through micro cracks from pressure release. Increasing porosity is usually associated with decreasing thermal conductivity (Schön, J, 2011).

4.6.2 Mineralogy

The controlling factor of conductivity in igneous rocks and metamorphic rocks is closely related to the dominant mineral phases and the density of the rock type (Birch & Clark, 1940, Sundberg et al., 2009). Common crystalline rock forming minerals have different physical properties depending on its specific chemical composition and atomic arrangement in the lattice. The relative proportions of minerals in different kinds of rock types will therefore yield different values for thermal properties such as thermal conductivity and heat capacity (Sundberg et al, 2009). Quartz has been reviewed by Horai (1971), Horai and Simmons (1969), Clauser & Huenges (1995), and Birch & Clark (1940) to have high or extremely high conductive ability in comparison to other common minerals. Felsic rocks will therefore generally tend to have relatively high thermal conductivity due to their higher content of quartz (Schön, 2011). Other common minerals that overall have prominent thermal conduction are mafic minerals and ore minerals (e.g. pyroxenes, olivine, magnetite, hematite and pyrite) as they have higher density than common felsic minerals (Sundberg et al., 2009).

Thermal conductivity of general rock types and specific mineral phases has traditionally been examined with direct laboratory measurements, both at room temperature at surface pressure and at elevated temperature and pressure (exceptions are well-log measurements in the KTB investigations or investigations in the oil and gas industry). Clauser & Huenges (1995) along with several authors argue that the thermal properties of rocks, and indirectly minerals, display a clear relationship of decreasing thermal properties (up to 60% decrease of the initial value) at elevated temperatures (above 300 °C). Reduction of thermal properties due to elevated temperature is not always the case in all rock types. High content of plagioclase feldspar can make the rock respond differently with increasing thermal conductivity (Birch & Clark, 1940; Clauser & Huenges, 1995). Thermal conductivity also has a tendency to increase with increasing magnesium content compared to iron in certain silicate minerals, where e.g. the olivine endmember forsterite exhibits higher thermal conductivity than fayalite (Birch & Clark, 1940).

4.6.3 Metamorphism and anisotropy

Rock anisotropy (i.e. foliation and/or lineation) is a factor that affects thermal conductivity (Sundberg et al., 2009). Metamorphic rocks with a strong preferred orientation (foliation) due to alignment of micas and amphiboles will inflict anisotropy also in the thermal conductivity. Laboratory measurements (See TPS-hot disk section) performed parallel with the direction of foliation generally yield higher values (up to 40 % higher according to Adl-Zarrabi et al., 2008) than perpendicular to the foliation (Clauser & Huenges, 1995). Anisotropy may also be considered as a factor in more prominent conductive mineral such as quartz. Quartz can display twice as high thermal conductivity parallel along the c-axis than along other perpendicular axes (Clark, 1966). It is therefore of great importance to take anisotropy of a rock into account when conducting experiments analyzing thermal properties. Metamorphism or other chemical and mineralogical alteration may change previous minerals into new minerals with different and even

greater conductive abilities. An example is the alteration of mafic minerals into chlorite, talc or serpentine (Sundberg et al., 2009).

Table 2. Measured values of thermal conductivity and specific heat capacity for different rock types (modified after Schön, 2011).

Rock	Thermal conductivity [W/m K]	Specific heat capacity [J/kg K]
Igneous rocks		
Granite	1.25-4.45 (mean = 3.05)	670-1550
Granodiorite	1.35-3.40 (mean = 2.65)	840-1260
Diorite	1.72-4.14 (mean = 2.91)	1130-1170
Syenite	1.35-5.20 (mean = 2.31)	-
Gabbro	1.62-4.05 (mean = 2.63)	880-1130
Diabase	1.55-4.30 (mean = 2.64)	750-1000
Basalt	1.40-5.33 (mean = 1.95)	880-890
Metamorphic rocks		
Quarzite	3.10-7.60 (mean = 5.26)	710-1340
Amphibolite	1.35-3.90 (mean = 2.46)	-
Gneiss (perpendicular schistosity)	1.20–3.2 (varying mean)	460-920
Gneiss (parallell schistosity)	1.20–4.19 (varying mean)	-

4.6.4 Theoretical models of thermal conductivity

Birch & Clark (1940), among others, investigated thermal properties of rock specimens with known mineralogical composition as well as single-mineral crystals by measuring the temperature response directly with a specially designed heater (thermopile). They later argued that thermal conductivity theoretically could be estimated in a rock by knowing parameters such as the modal composition of the rock and the specific conductive abilities of common minerals in the rock. This approach resulted in Equation 6, which assumes that thermal conductivity is parallel relative to mineral phases in a sample. $\lambda_{parallel}$ is the bulk thermal conductivity parallel to the sample, *n* is the fractional volume of a specific mineral phase and *k* the conductivity of a specific mineral (an arithmetic mean by weighting the volume fraction).

$$\lambda_{parallel} = \sum n_1 * k_1 \qquad (6)$$

Their experiments revealed that the postulated calculation was in good agreement with their measured values of thermal conductivity, and that some minerals are better conductors in specific optic axis (Birch & Clark, 1940). It should be noted that the parallel equation is often described to display the over boundary of a rock type's thermal conductivity (Sundberg et al., 1985, Clauser & Huengens, 1995) but is reviewed by Sundberg et al. (1985) to work relatively better than several other common theoretical equations for thermal conductivity.

Horai & Simmons (1969), Horai (1971) and Horai & Baldridge (1972) performed extensive thermal conductivity measurements of 119 single-phase minerals by pulverizing the minerals (with monomineralic composition) into a homogenous aggregate powder (less than 0.05 mm according to Horai, 1971). The aggregates were separately added into distilled water as a mixture

and were measured by using the needle-probe method (Herzen & Maxwell, 1959). Table 3 displays a brief compilation of four different data sets with literature values for thermal conductivity. Values from Cermak & Rybach (1982) and Clauser & Huenges (1995) have been collected with varied methods (single crystals, aggregate powder, etc.) to obtain values and are therefore only used for display compared with values of Horai (1971). The obtained thermal conductivity from the multiple mineral phases in the study was then inserted into the Hashin & Shtrikman equation (1962), which calculated thermal conductivities for different theoretical whole rocks (Baldridge & Horai, 1972). This equation was intended for sedimentary rocks and unconsolidated material, which was argued to work well with the pulverized minerals that Horai (1971) and Baldridge & Horai (1972) utilized (Sundberg et al., 1985). Balridge & Horai (1972) claimed that the method generated an average error of 5% compared to measured values, which indicated that the values for mineral conductivity were credible. The information provided by Horai & Simmons (1969), Horai (1971) and Balridge & Horai (1972) can be utilized in Equation 6 (as well in other equations not shown in this report) to approximate the thermal conductivity of igneous and metamorphic rocks with known modal composition as an option to direct measurements.

Table 3. Thermal conductivity (W/mK) from literature after minerals found during optical microscopy and SEM investigations. Values of Cermak & Rybach (1982) were retrieved through a compilation of Schön (2011).

Mineral phases	**Clauser & Huenges (1995)**	**Cermak & Rybach (1982)**	**Horai & Simmons (1969)**	**Horai (1971)**
Quartz	7.69	7.69	7.68	7.68
K-feldspar	2.04-2.49	2.31-2.49	2.37-2.42	2.31-2.6
Plagioclase	2.0-2.34	1.68-2.31	1.68-2.35	-
Biotite	2.02	-	1.7-2.34	1.7-2.34
Muscovite	2.28	2.32	2.21-2.49	2.21-2.49
Hornblende	2.81	-	2.54	2.54-3.07
Ca-clinopyroxene	4.23-4.66	-	3.82	3.82
Chlorite	5.15	5.14	-	4.26-6.18
Titanite	2.34	2.33	-	-
Magnetite	5.1	5.1	5.1	5.1
Ilmenite	2.38	-	2.2	2.2-2.55
Calcite	3.59	-	3.59	3.59
Apatite	1.38	1.37	1.37-1.38	1.37-1.38
Andradite	-	-	3.09	3.09

5. Methods

5.1 Sample collection and preparation

The samples of this study were chosen specifically to display differences in thermal conductivity and heat capacity of different rock types, with relatively varying mineralogical compositions.

One block of diameter ~ 20 cm was collected from each of the six rock types in the five quarries (Figure 2-3, Table 4), located within the provinces of Västergötland, Småland and Halland. Each block was cut with diamond saw equipment at CBI, producing thermal conductivity specimens of the dimensions 12 x 10 x 5 cm (Figure 4-5). The Bårarp block was cut in two separate 12 x 10 x 5 cm specimens from the same block in two different directions (parallel and perpendicular) according to foliation. A two cm thick slab was cut from each of the thermal conductivity specimen (yielding final specimen size 10 x 10 x 5 cm) and was sent for thin-section preparation. The slab was cut so that the thin section is parallel with the heat transfer direction in the later TPS tests. The pieces (Bårarp having two pieces) were later ground and polished in the normal order for thin-section preparation and ended up 25-30 micron thick (Figure 6).

Table 4. The different quarries where aggregate samples were collected, their relative location, and rock type addressed by the quarry owners.

City landmark	Quarry name	Owner	Rock type
Jönköping	Forserum	Skanska	Quartzite, Diabase
Lidköping	Gillstad	Swerock	Gabbro
Västervik-Oskarshamn	Flivik	Emmaboda Granit AB	Granite
Uddevalla	Fröland	Swerock	Granite with pegmatite
Halmstad - Falkenberg	Bårarp	Emmaboda Granit AB	Granitic Gneiss

Figure 2. Sample blocks collected at the Forserum quarry.

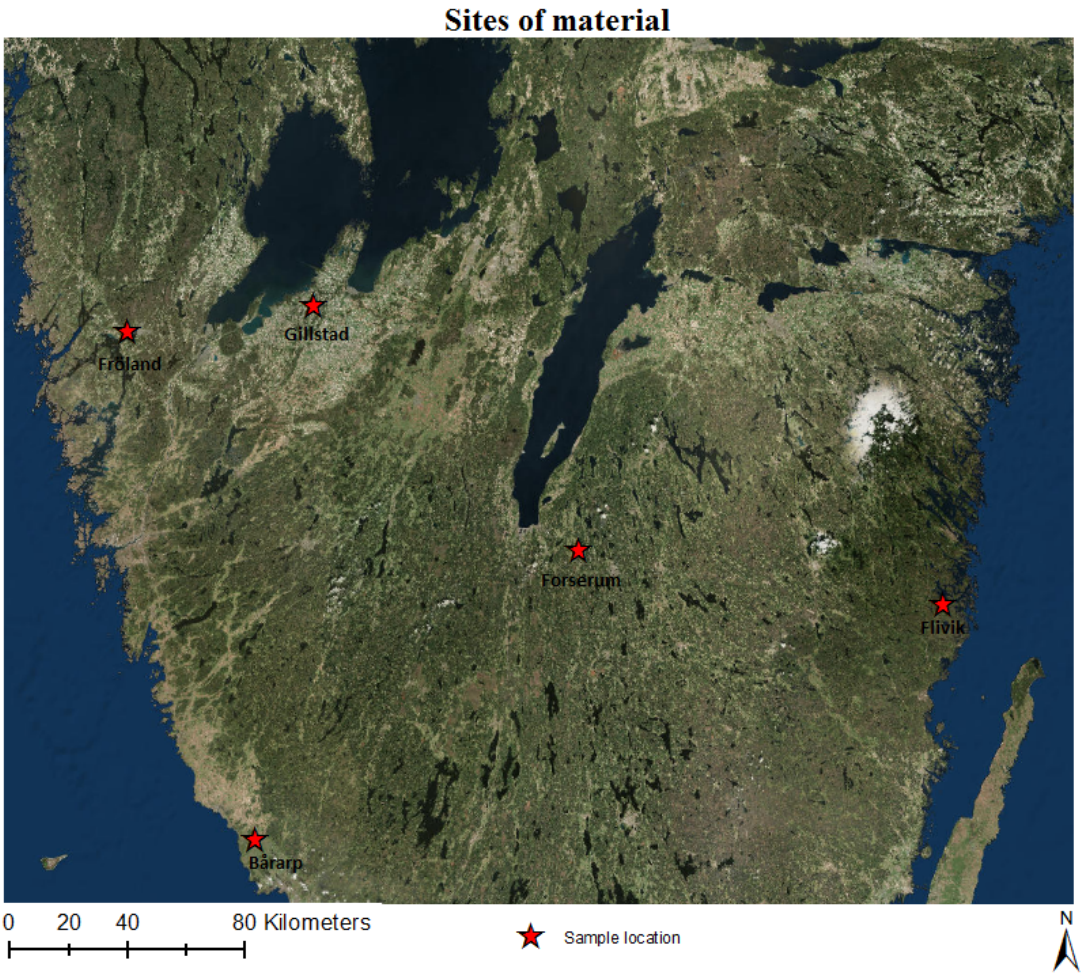

Figure 3. GIS-map (Swereff 99 TM) showing the regional location of the different quarries where the blocks were collected (©ESRI).

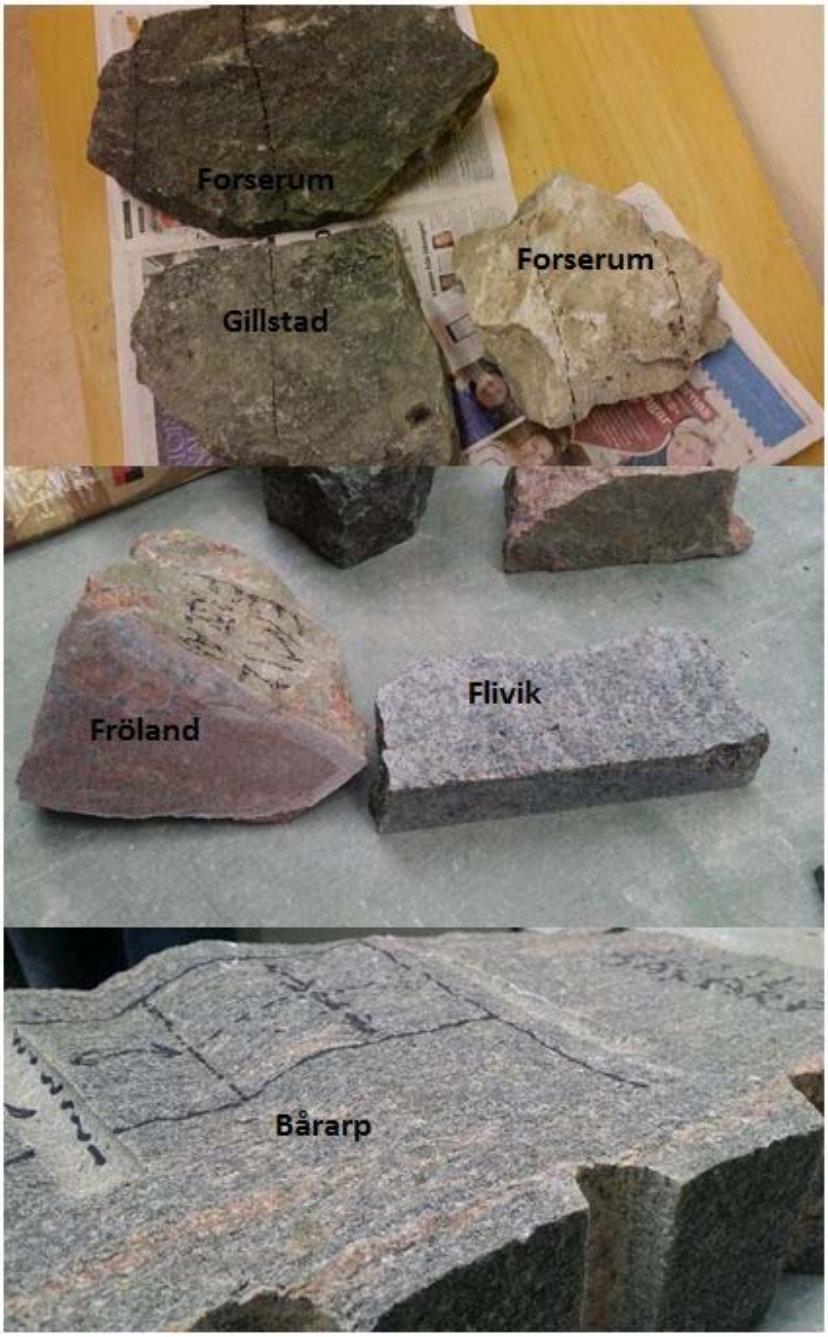

Figure 4. All six samples chosen for TPS-measurement and thin-section preparation.

Figure 5. Four of the samples cut into the dimensions of 10 x 10 x 5 cm.

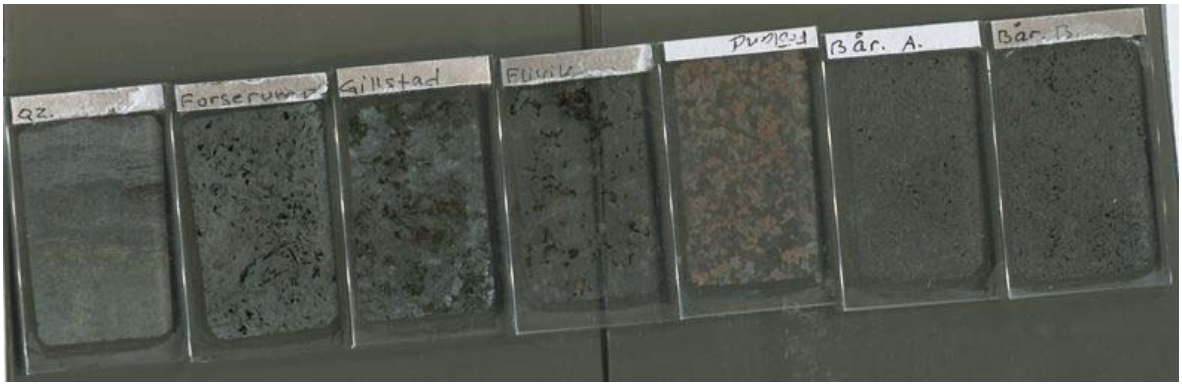

Figure 6. The thin sections from the seven specimens (note that the Bårarp specimen on the right side was divided into two thin sections).

5.2 Hot Disk TPS measurements

Thermal properties of the prepared 10 x 10 x 5 cm specimens were measured at SP Fire Research with the Hot Disk laboratory equipment. The specimens were cut in half and polished by a rotating diamond-reinforced surface. The polishing stage creates a complete flat surface with full contact with the TPS-probe sensor surface. As a standard procedure, the specimens were conditioned at 22 °C for 14 days in order to dehydrate potential water from pores. Each specimen was mounted into the instrument, with the TPS-sensor placed between the two halves of the specimen, and constant forces of 140 N applied above and below to ensure full contact during the procedure (Figure 7).

The Hot Disk equipment utilizes a specific technique called the Transient plane source (TPS) which is a probe with a flat sensor consisting of two thin layers of Kapton (polyamide film) with a double-spiral made of nickel emplaced between the layers (Figure 7). The TPS works by passing an electric current through the nickel spiral which increases the temperature inside the TPS during a short period of time. The resulting heat will then be transported through the material of interest according to its internal properties (Figure 7). The sensor measures the response of temperature over time which can be used to calculate thermal conductivity and heat diffusivity (Hot Disk Instrument, 2015). Heat capacity is obtained by dividing the measured thermal conductivity with the thermal diffusivity according to the relationship of Equation 5.

The technique was invented and validated by Gustafsson (1991) and has been reviewed by several authors (e.g. Adl-Zarrabi et al., 2009) to yield replicative and credible data for a wide range of materials and liquids, including rock samples. The Hot Disk TPS equipment is designed to measure a wide span of thermal conductivity inside different material from 0.005-1800 W/m K (Hot Disk Instrument.se). The specific setup chosen in this case was the 5501 sensor (Kapton film) with a radius of approximately 6.403 mm and a constant effect of 700 mW, which was applied during 20 seconds in 5-29 intervals for each sample (see appendix for each specimen and specific data). After each 20 seconds measurement, the TPS pauses for 30 minutes before taking next systematical measurement. The chosen analysis module in the software for the setup was the “bulk module”, which measures the sample radially.

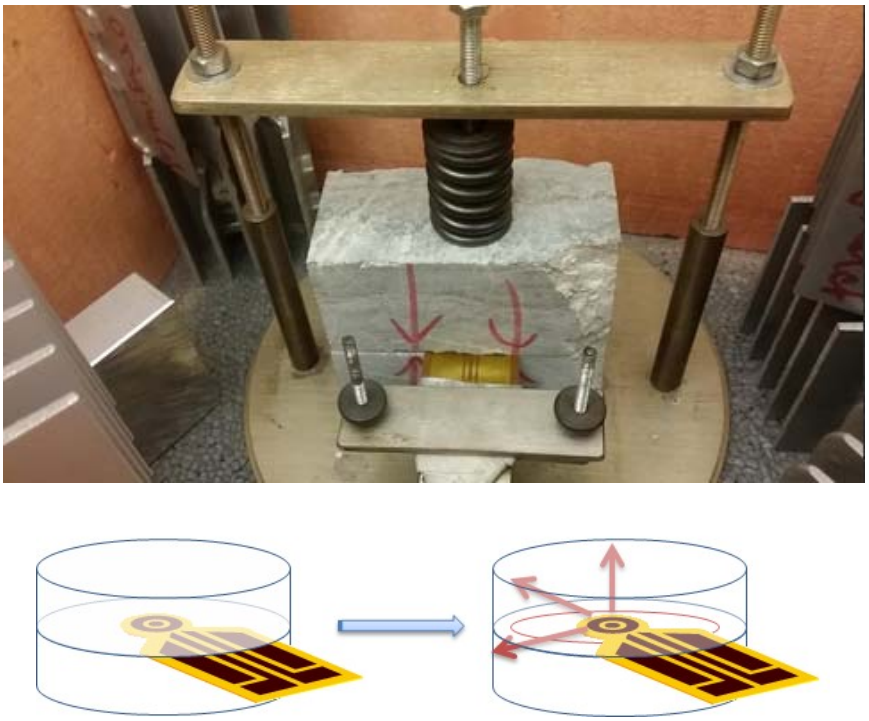

Figure 7. Schematic of the TPS-sensor setup being inserted in between the cut and polished rock surfaces (Forserum quartzite in this case) with an applied pressure. The lower schematic shows how energy transfers inside the cube from the TPS- sensor (Kapton variant).

5.3 Petrographic analysis

5.3.1 Optical microscopy

The thin sections were investigated with two different optical microscopes (Leica DMLP and Leica DMRXP) in order to acquire information about the petrography of the samples, where both plane light (PPL) and cross-polarized light (XPL) was utilized in the normal procedure for optical microscopy. The thin sections were photographed with an Olympus DP71camera during analysis and also scanned and digitalized with polarization film in a normal scanner to facilitate SEM analysis. The microscope was used to investigate bulk mineralogical composition (by point counting), textures and average grain size (by measuring the dimensions with the microscope camera). Results from the optical microscopy and SEM are presented in the result section.

5.3.2 Point counting (mineral mode)

The thin sections were counted with a Stepping-stage machine from PetrogLite (Figure 8), which was mounted on the Leica DMRXP. The Stepping stage moves the thin section systematically to ensure representative distribution of spots across the thin section. Information regarding the dimensions of the thin section, the coordinates for the area of interest and the desired total amount was inserted into the PetrogLite V2.35, where it calculated the volume fraction of each

mineral phase according to the number of spots. In order to gain statistical credibility, 750 points were counted in each thin section. At some occasions, the stepping-stage had problems moving the sample correctly due to the holder clasp of the machine (Figure 8), but this was compensated for by adding points to the count. Some of the thin sections had matrix or groundmass, which was hard to distinguish as a single mineral during point counting and was simply denoted *matrix*. The modal distribution of phases in the matrix was estimated by general petrography. Accessory phases (i.e. <1%) was not accounted for in the calculation due to little significance for the project.

Figure 8. The stepping-stage mounted onto the Leica DMRXP optical microscope.

5.3.3 SEM analysis

The thin sections were carbon coated and analyzed with the SEM (Scanning Electron Microscope) at the Department of Geology at the University of Gothenburg. The SEM (Hitachi S-3400N) was equipped with an Energy-Dispersive X-ray spectrometer (Oxford Instruments X-Max EDS). Working distance varied between 9.5-10.5 mm during measurements, operating current at 20 eV with the probe current set approximately at 6 nA. The thin sections were analyzed to gain information about certain mineral phases and to identify undistinguishable mineral phases such as opaque minerals, accessory minerals and minerals within the matrix.

5.4 Calculations and analytical work

Thermal conductivity in all specimens was calculated by using the volume fraction from point counting together with Equation 6 and the average mineral thermal conductivity values in Table 5, after Horai (1971). A new addition to Table 5 is that K-feldspar is divided into orthoclase and microcline polymorphs whereas plagioclase is divided into compositions of albite ($Ab_{89}An_{11}$) and labradorite ($Ab_{46}An_{54}$). This was done to adjust for the different feldspar compositions in felsic and mafic rock types with intermediate composition. Titanite was not addressed in either tabulated values of Horai & Simmons (1969) or Horai (1971), and was therefore taken from Clauser & Huenges data (1995). The calculated values for thermal conductivity were plotted with the measured conductivity values for all specimens. The calculated and measured values for

thermal conductivity were plotted with the quartz content in each specimen. The calculated and measured values were furthermore against grain size. The average grain size was measured in five of the seven specimens (See Appendix 4-8 for grain sizes), which were divided into two groups based on felsic mineralogy (Flivik, Fröland and Bårarp B) and mafic mineralogy (Gillstad and Forserum), and thereafter plotted against thermal conductivity.

The values for heat capacity were chosen from Table 6, where either a single value for heat capacity or an average of two values was used depending on the availability. The values were then converted from specific heat capacity to volumetric heat capacity by utilizing average mineral density data (www.webmineral.com) according to Equation 4 (see Appendix 1-2). The conversion was performed in order to compare calculated results with the TPS results. It should be noted that information about some minerals (titanite and andradite) is not present in the Tables 5 and 6 because they were not specifically addressed in the original data. The calculated volumetric heat capacity was plotted with the TPS data and the data of average mineral grain size in all five of the specimen (see Appendix 4-8).

Table 5. Thermal conductivity values (W/mK) from Horai (1971) utilized for calculations (slightly modified from Table 3 to address different feldspars in the specimens).

Mineral phase	**Horai (1971) values**
Quartz	7.68[1]
Microcline	2.34[1]
Orthoclase	2.31[1]
Plagioclase-Oligoclase (Ab_{89}-An_{11})	1.98[1]
Plagioclase-Labradorite (Ab_{46}-An_{54})	1.52[1]
Muscovite	2.3[2]
Biotite	2.02[2]
Hornblende	2.8[1]
Augite	3.82[1]
Chlorite	4.9[2]
Titanite	2.34[3]
Magnetite	5.1[2]
Ilmenite	2.37[2]
Calcite	3.59[2]
Apatite	1.37[2]
Andradite	3.09[1]

1 indicates single value, 2 indicates average value and 3 indicates borrowed due to being absent in original data.

Table 6. Specific heat capacity values (kJ/ kgK) from literature for each mineral found during optical microscopy and SEM investigations. Values were retrieved through compilation of Schön (2011).

Mineral phases	Melnikov et al. (1975)	Cermak and Rybach (1982)	Values
Quartz	0.74	0.7	0.72[2]
K-feldspar	0.63	0.68	0.65[2]
Plagioclase	-	0.71	0.71[1]
Biotite	-	0.76	0.76[1]
Muscovite	-	0.78	0.76[1]
Hornblende	0.75	-	0.75[1]
Augite	0.67	0.69	0.68[2]
Chlorite	0.6	-	0.61[1]
Titanite	-	-	-
Magnetite	0.6	0.6	0.6[2]
Ilmenite	0.77	-	0.77[1]
Calcite	0.5-0.52	0.5	0.51[1]
Apatite	0.8-0.83	0.79	0.81[1]
Andradite	-	-	-

1 indicates where single values were used and 2 indicate where average values were used during calculations.

6. Results

6.1 Hot Disk measurements

The results from the Hot Disk TPS measurement yielded varied values and properties among the different specimens, and these can be viewed in Table 7 and Figure 9. Table 7 and Figure 9 display the relationship of thermal conductivity and diffusivity (according to the relationship of Equation 3 and Equation 5), where the volumetric heat capacity is controlled by the ratio between thermal conductivity and diffusivity changes. It can be observed that the mafic samples, and especially the diabase one, have the highest value for volumetric heat capacity. The mafic specimens also have very similar values in thermal conductivity compared to the granites. The Fröland specimen displays the highest value for thermal conductivity, but also has the highest value for diffusivity at the same time. The Bårarp specimens A and B have low thermal conductivity compared to all specimens other than the diabase, together with the lowest values for heat capacity for all specimens. The greatest difference in thermal conductivity can be observed between the Fröland granite and the Forserum diabase (36% higher in the Fröland specimen). The greatest difference in diffusivity is evident between Fröland and the diabase (38%). Specific heat capacity displays a 25% difference between the diabase and Bårarp A. The Forserum quartzite displays the greatest anomaly of thermal properties compared with the rest of the samples in Figure 9.

Table 7. Results from the Hot Disk TPS measurements showing the average values of thermal conductivity, diffusivity and specific heat capacity of all seven specimens (Bårarp is displayed as two specimens).

Specimens	**λ (W/mK)**	**α (mm²/s)**	***Cv* (MJ/m³K)**
Forserum quartzite	3.34	1.50	2.26
Forserum diabase	2.46	1.02	2.42
Gillstad	2.58	1.11	2.32
Flivik	3.05	1.34	2.27
Fröland	3.82	1.64	2.33
Bårarp A	2.48	1.36	1.83
Bårarp B	2.53	1.21	2.09

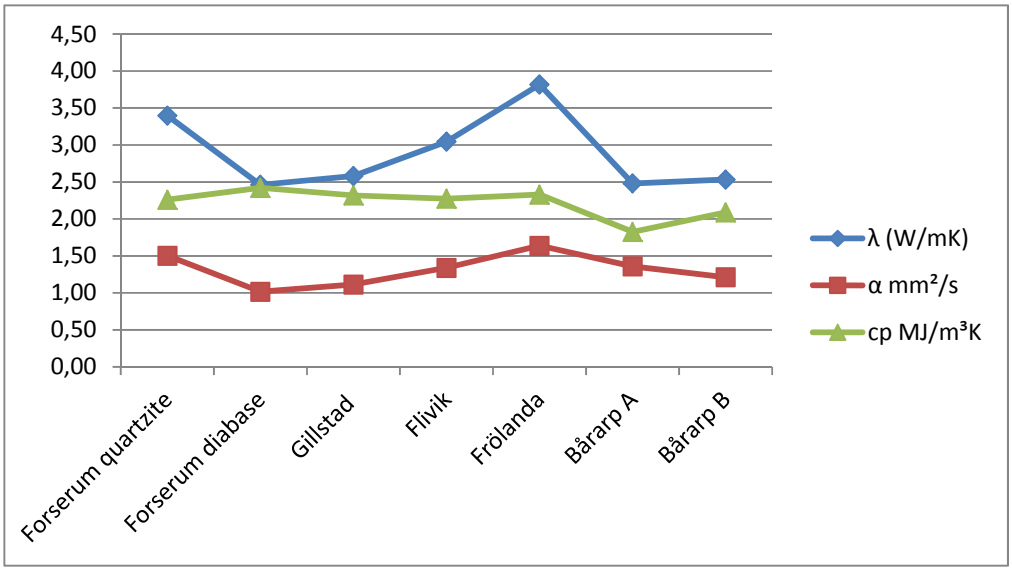

Figure 9. Graph showing values from the TPS-measurements on all of the seven thermal conductivity specimens (Bårarp is presented as two separate specimens). Note that the y-axis includes all three different thermal properties values and units: (W/mK), (mm²/s) and (MJ/m³K) for all specimens.

6.2 Petrographic analysis

Forserum – quartzite

In hand sample, the rock is white to grey, equigranular, fine grained and structurally anisotropic with distinct straight banding (similar to marble texture) with no visible external alteration products or weathering. The main modal phases in the thin section are calcite, quartz, plagioclase and garnet (Table 8) with accessory phases of apatite and possibly wollastonite. The mineral phase denoted as garnet is optically isotropic in XPL (cross polarized light) and has yellow to

brown color in PPL (plane polarized light) (Figure 12a-d). After SEM analysis (Figure 13b and Table 9), the garnet phase was recognized to consist of Ca, Si, Fe and Ti, which might support a Ca-Fe-Ti type garnet (a possible solution of andradite and other Ti-bearing garnets). SEM analysis also revealed that calcium silicates are present in the sample (possibly wollastonite due to the Si-Ca relationship) although they could not be precisely identified in the thin section.

The sample is overall inequigranular with uneven grain boundaries. Calcite grains sizes are 2.2-0.03 mm in longest dimension and anhedral. Quartz grains sizes ranges from 0.65-0.02 mm and are subhedra to anhedral with partly undulose extinction. Plagioclase grain size ranges from 0.6-0.04 mm in longest dimension and have subhedral grain shape. Garnet grain size ranges from 0.2-0.02 mm and are subhedral in grain shape. Certain surfaces in the thin section are dominated by a fine-grained matrix (Figure 11c-d), that has undistinguishable grain boundaries and is estimated to consist of 50% calcite, 20% plagioclase, 20% quartz and 10% garnet. The matrix tends to grade into accumulations of the same mineralogy (calcite or quartz, plagioclase). The mineral grains in the accumulation occur oriented in the same direction (possible banding texture) with subhedral-anhedral grain shapes with more distinctive boundaries. Plagioclase has characteristic polysynthetic twinning and can occur in an interfingering texture between calcite accumulations (Figure 10b). Apatite also tends to appear between the larger calcite grains and also occasionally in the matrix. The mineral composition in the thin section (low amount of quartz, high amount of calcite together with calcium silicates and possible garnet) does not describe a traditional quartzite, but instead a skarn-like rock. The specimen will therefore be called skarn in the discussion section.

Table 8. Forserum quartzite thin section. Result of the point counting with major mineral phases and their respective volume fraction distribution. Certain mineral phases could not specifically be distinguished during microscopy and were therefore called matrix.

Mineral phases	**Points counted**	**Volume fraction (%)**
Quartz	164	21
Plagioclase	110	14
Calcite	241	31
Garnet	51	6
Matrix	220	28
Totals	786	100

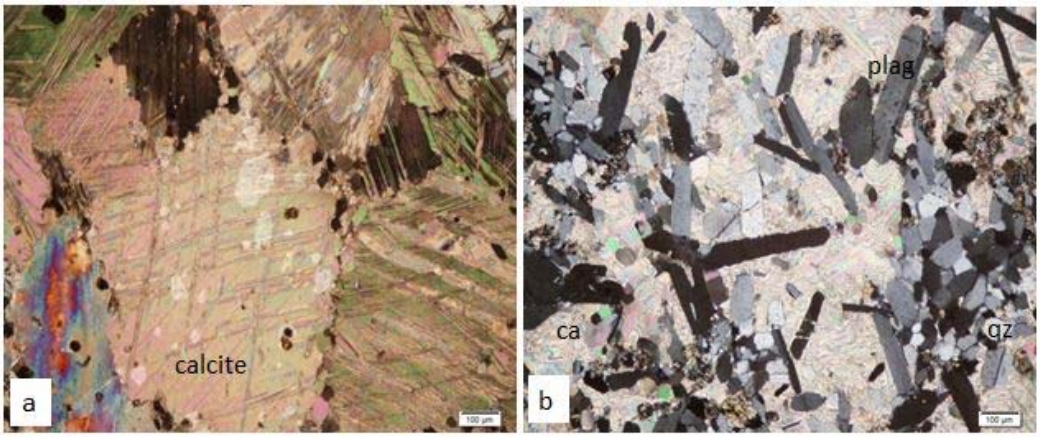

Figure 10. Photomicrographs of the Forserum quartzite thin section. ***(a)*** *Large calcite grains (XPL)* ***(b)*** *shows the interfingering of plagioclase and also quartz between the larger adjacent calcite grains (XPL). The white scale bar in the right lower corner represents 100 microns.*

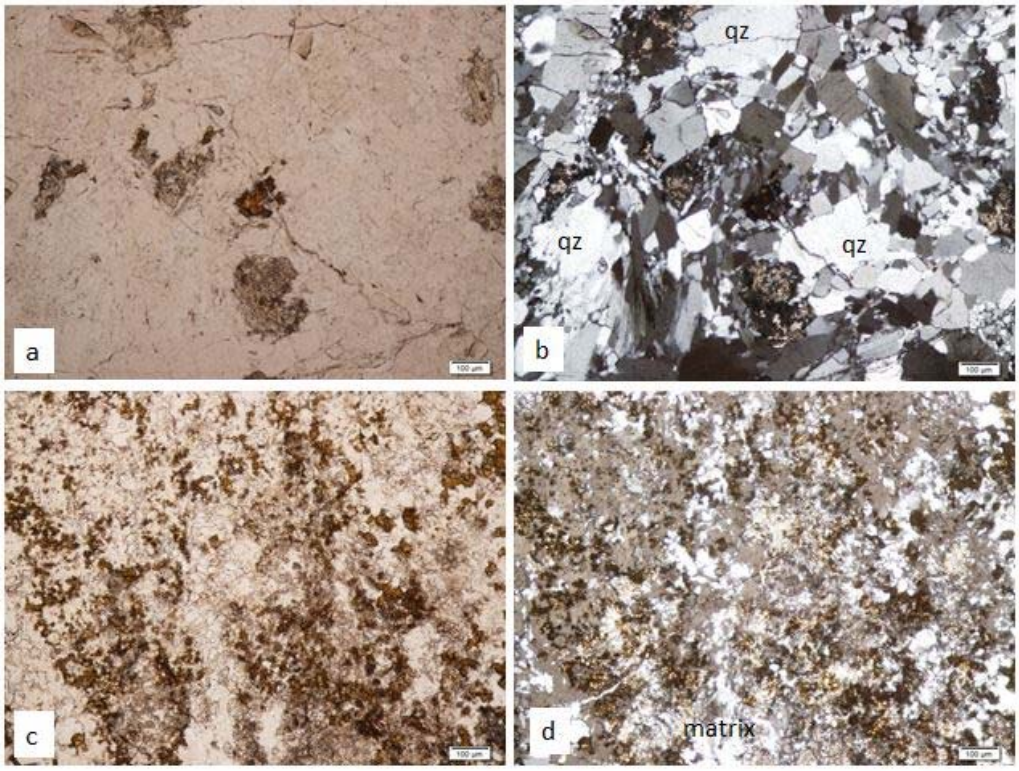

Figure 11. Photomicrographs of the Forserum quartzite thin section. ***(a-b)*** *Show the accumulation of quartz (banding) in PPL (left) and XPL (right) where the scale bar in the right lower corners represents 100 microns.* ***(c-d)*** *Show the matrix in the sample where the scales bar in the right lower corner represents 100 microns.*

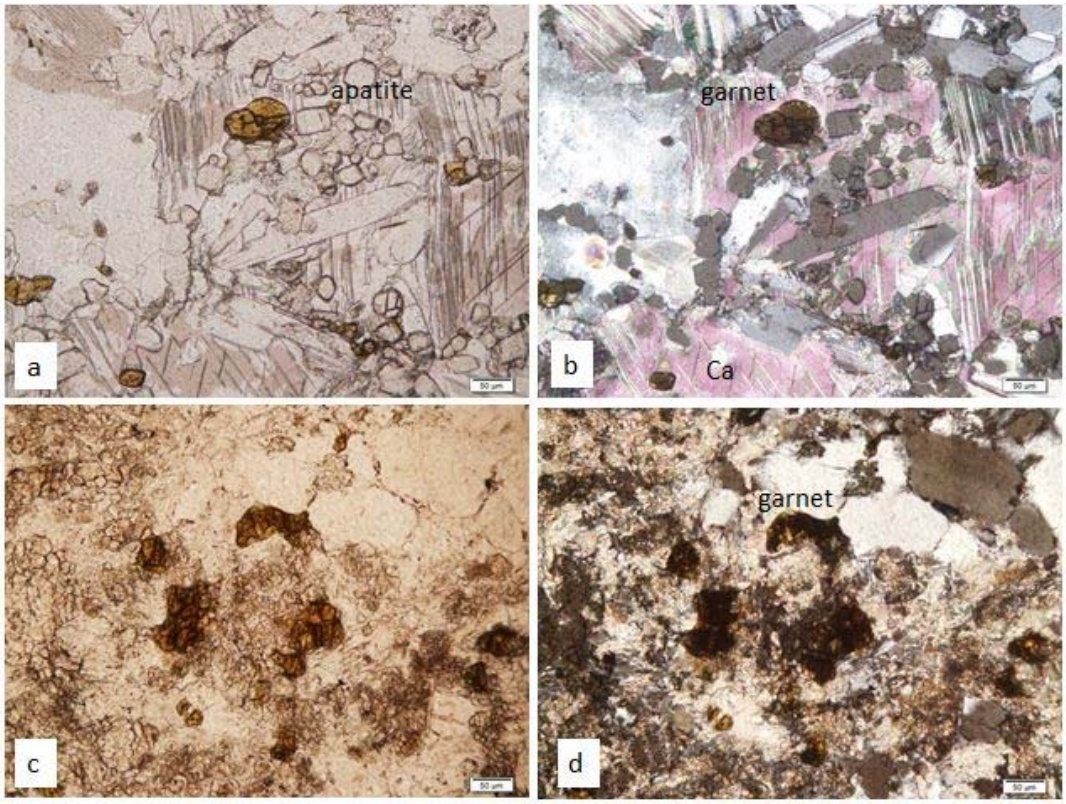

*Figure 12. Photomicrographs of the Forserum quartzite thin section. Images **(a-d)** show the garnet found in the thin section, where images left are PPL and right are XPL. Scale bar in the right lower corner represents 50 microns.*

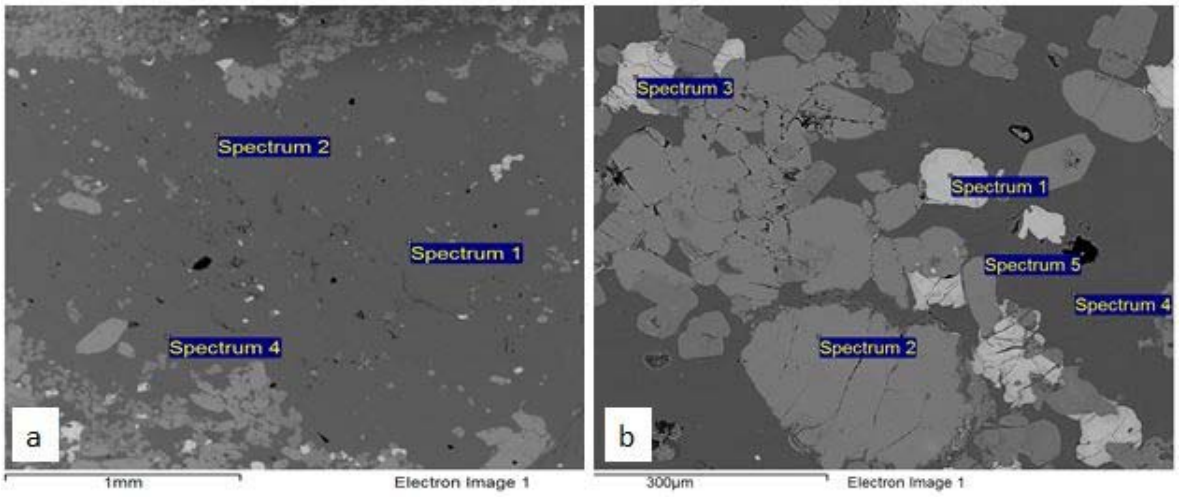

*Figure 13. Forserum quartzite specimen. **(a)** An area of a SEM analysis, where spectrum 1-4 are all calcite. **(b)** Spectrum 1 is interpreted as garnet, spectrum 2 is interpreted as wollastonite and spectrum 4 is calcite.*

Table 9. Forserum quartzite specimen. EDS analysis connected to Figure 13b, where spectrums 1 & 3 refer to the mentioned garnet composition and spectrum 2 refers to the wollastonite.

Element	Spectrum 1 weight%	Spectrum 2 weight%	Spectrum 3 weight%
Mg	0.12		0.1
Al	1.57		1.54
Si	12.12	22.03	11.77
Ca	21.04	31.3	20.4
Sc	0.32	0.28	0.29
Ti	3.83		3.63
V	0.13		
Fe	15.4		14.85
Zr	0.22		0.28
I	0.57		0.56
O	45.66	60.03	46.43
Totals	100.98	113.64	99.85

Forserum – diabase

In hand sample the diabase is dark gray, inequigranular, isotropic, medium grained and massive with visible cracks and features of red minerals near the cracks. The thin section mainly consists of plagioclase, augite and ilmenite and minor phases of apatite and chlorite (Table 10). The sample has inequigranular grain size distribution. Plagioclase grain size ranges from 4.5-0.2 mm in longest dimension, and grains are subhedral. Augite (clinopyroxene) grains ranges from 1.8-0.1 mm in longest dimension and are subhedral. Ilmenite grain size ranges from 2.5-0.1 mm in longest dimension and have subhedral and flaky grain shapes that tend to be oriented in two main directions. Apatite may appear as free subhedral grains or needle-shaped grains within other minerals (Figure 15b) ranging from 0.5-0.05 mm in longest dimension. Plagioclase grains can be coarse and display gabbro texture together with adjacent clinopyroxenes (Figure 14a). The thin section has microscopic cracks systematically (Figure 14b) running across the entire sample, which have a close resemblance to cataclastic texture. The cracks have a gray brown groundmass with potentially 50% recrystallized K-feldspar (probably adularia) identified through SEM analysis (Figure 15c, Table 10). The groundmass inside the cracks contains larger clasts of fragmented plagioclase (25%) and clinopyroxene (25%) with occasional ilmenite and chlorite. Minerals in the sample overall seem to have been altered during low-grade metamorphism. Augite is at some places altered by chlorization where larger areas inside a grain or around the boundary of the grain (reaction rims or coronas) may be replaced. Plagioclase seems to be affected by minor seritization or possibly dispersed clinopyroxenes within small cracks inside the grains.

Table 10. Forserum diabase specimen. Result of the point counting with major mineral phases and their respective volume fraction distribution. Certain mineral phases could not specifically be distinguished during microscopy and were therefore called fracture matrix.

Mineral phases	**Points counted**	**Volume fraction (%)**
Plagioclase	515	64
Ca-clinopyroxene	176	22
Ilmenite	71	9
Fracture matrix	37	5
Totals	799	100

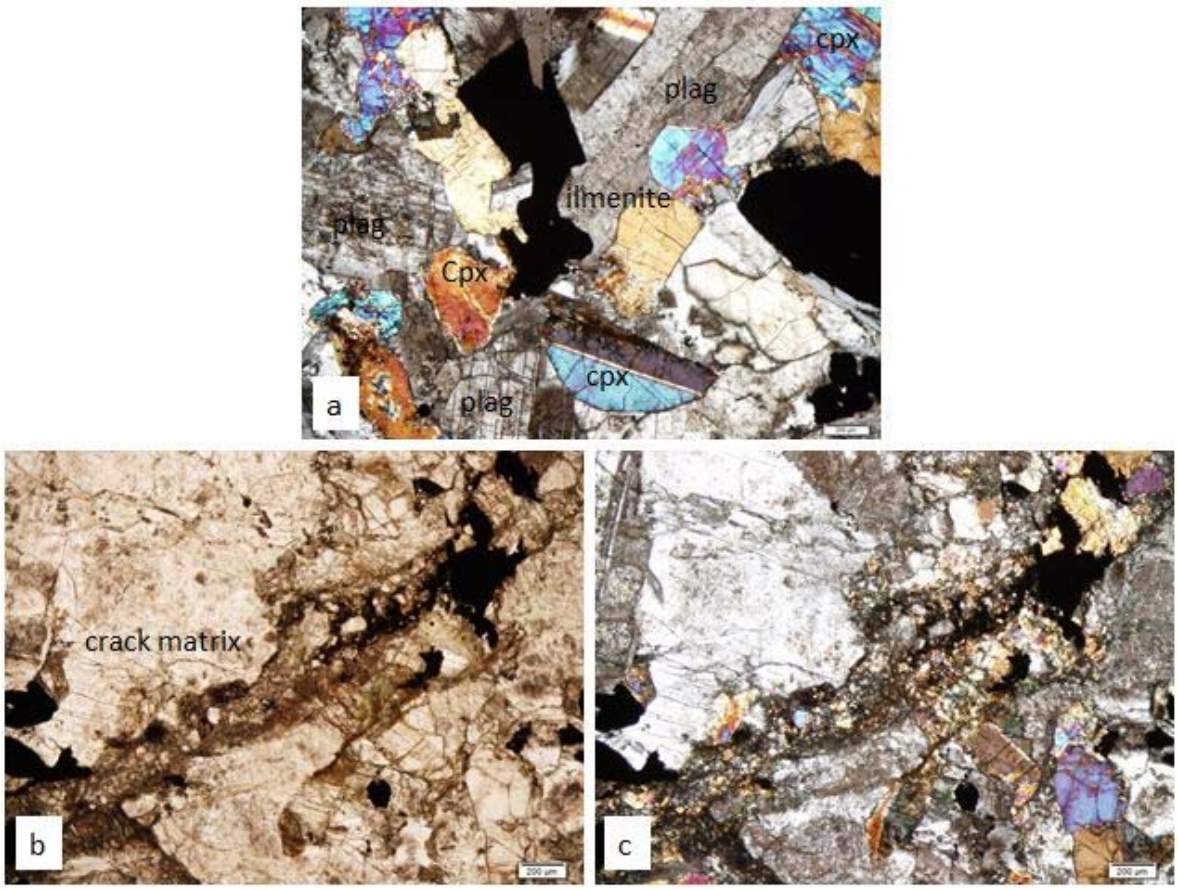

*Figure 14. Photomicrographs of the Forserum diabase thin section. Image **(a)** shows overall mineralogy in the sample with coarse plagioclase grains, smaller clinopyroxenes (augite) and opaque phases as ilmenite (XPL). Images **(b-c)** show the fracture matrix described in the text that runs across the sample with fragmented cliopyroxenes and plagioclase (left PPL and right XPL). The scale bar in the right lower corner on all images represents 200 microns.*

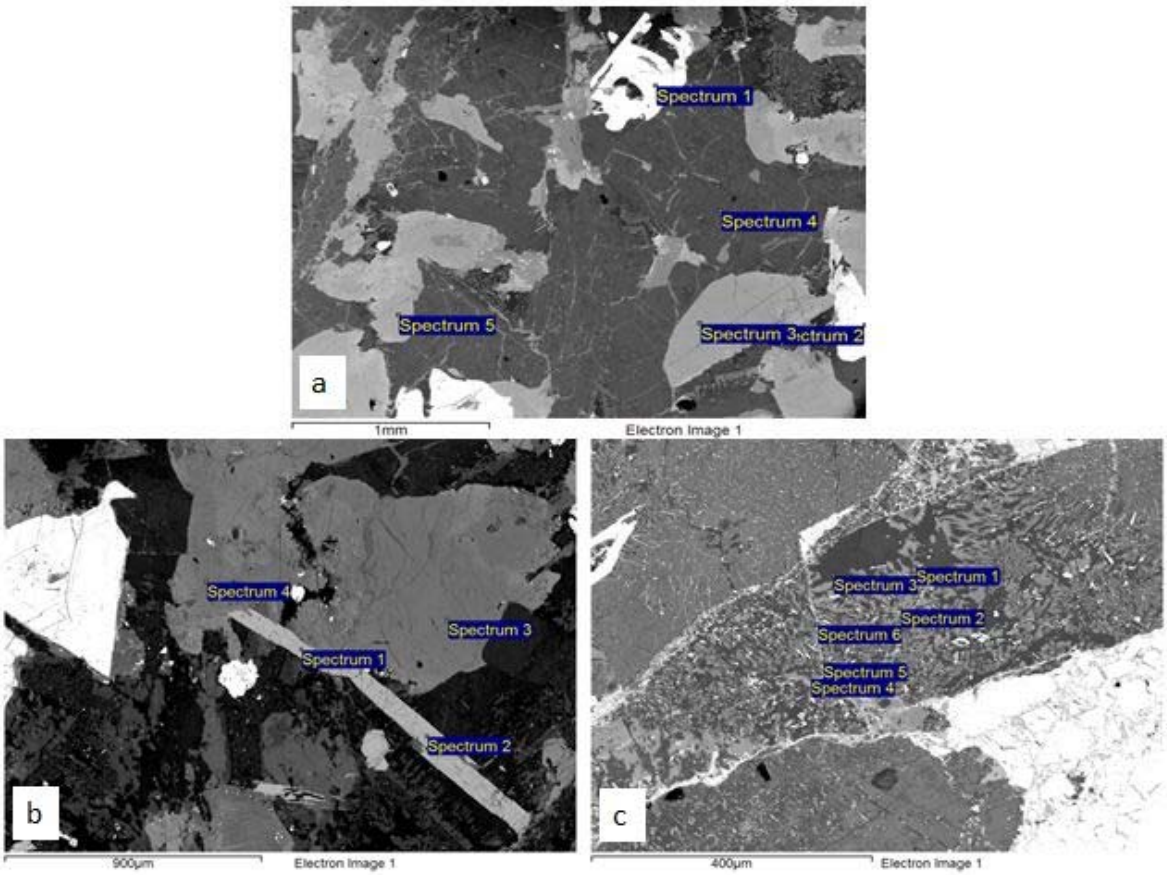

*Figure 15. BSE sites of SEM analysis in the Forserum diabase. Image **(a)** shows clinopyroxene augite (spectrum 3 & 5), plagioclase (spectrum 4) and ilmenite (spectrum 1), image **(b)** shows augite (spectrum 3-4) and apatite (spectrum 1-2) and image **(c)** shows the fracture matrix where most spectrums are K-feldspar or adularia (1-4).*

Table 10. Forserum diabase specimen. EDS analysis connected to the same site as Figure 15c. Notice the relatively high presence of potassium in the analyses.

Elements	Spectrum 1 wt %	Spectrum 2 wt %	Spectrum 4 wt %
Na	0.32	0.17	0.31
Al	9.51	6.21	9.43
Si	29.73	34.89	29.75
Cl			0.14
K	12.95	8.43	12.91
Fe	0.1	0.1	0.09
Ti		0.2	0.36
O	45.12	47.18	45.19
Totals	97.72	97.18	98.19

Gillstad – gabbro

The Gillstad hand sample is dark gray to green, massive and medium grained with slight foliation texture due to biotite and/or hornblende. The thin section consists of modal phases such as plagioclase, biotite, hornblende, clinopyroxenes (augite), quartz and magnetite (Table 11). The thin section also consists of a varying matrix with major phases of hornblende-amphibole, clinopyroxene and biotite as well as accessory apatite and epidote. Mineral grain sizes are inequigranular from very fine to medium-coarse grained due to the matrix with larger phenocrysts of plagioclase. Plagioclase is the most frequently occurring mineral phase in the Gillstad thin section where coarse grains often display gabbroic texture together with surrounding mineralogy. The matrix is estimated to consist of 50% amphiboles (mainly hornblende), 30% clinopyroxene, 10% biotite, 5% plagioclase and 5% quartz. Plagioclase grain sizes ranges from 4.5-0.1 mm in longest dimension (smaller while occurring in the matrix) with subhedral-anhedral grain shape. Clinopyroxenes grain size ranges from 2.1-0.05 mm in longest dimension (smaller in matrix) and are subhedral-andhedral in grain shape. Biotite, hornblende and apatite can appear as flaky (micaceous) or fibrous shapes both as single grains as well as in the matrix. Hornblende grain sizes ranges from 2.5-0.3 mm in longest dimension (smaller in matrix) whereas biotite grain sizes ranges from 0.1-0.05 mm. Biotite grains are slightly folded to folded in the thin section but can also grow in an interlocking pattern around plagioclase grain boundaries. Quartz occurs as smaller recrystallized subhedral grains in between larger plagioclase grains (Figure 16a) or in the matrix. Common features in the specific sample are alteration, exsolution texture and other replacement textures of clinopyroxenes due to possible metamorphism. Hornblende frequently grows around grain boundaries of clinopyroxens as either rim or coronas which suggest uralitization and that the hornblende may be secondary in some instances (Figure 16b). Pseudomorphs of former clinopyroxene grains are common in the thin section (Figure 17a). Chlorite and biotite can occasionally replace or grow around clinopyroxenes and amphiboles boundaries. Epidote grains are sometimes found growing inside plagioclase grains, at the grain boundary or between grain boundaries of plagioclase which may indicate possible saussuritization. The present mineral assemblage and textures in the thin section can be viewed as a gabbroic rock or possibly a metagabbro (in lower amphibolite facies).

Table 11. Gillstad mafic specimen. Result of the point counting with major mineral phases and their respective volume fraction distribution. Certain mineral phases could not specifically be distinguished during microscopy and were therefore called matrix.

Mineral phases	**Points counted**	**Volume fraction (%)**
Quartz	48	6
Plagioclase	422	55
Hornblende	80	10
Ca-clinopyroxene	34	4
Biotite	101	13
Alteration matrix	69	9
Magnetite	10	1
Totals	764	100

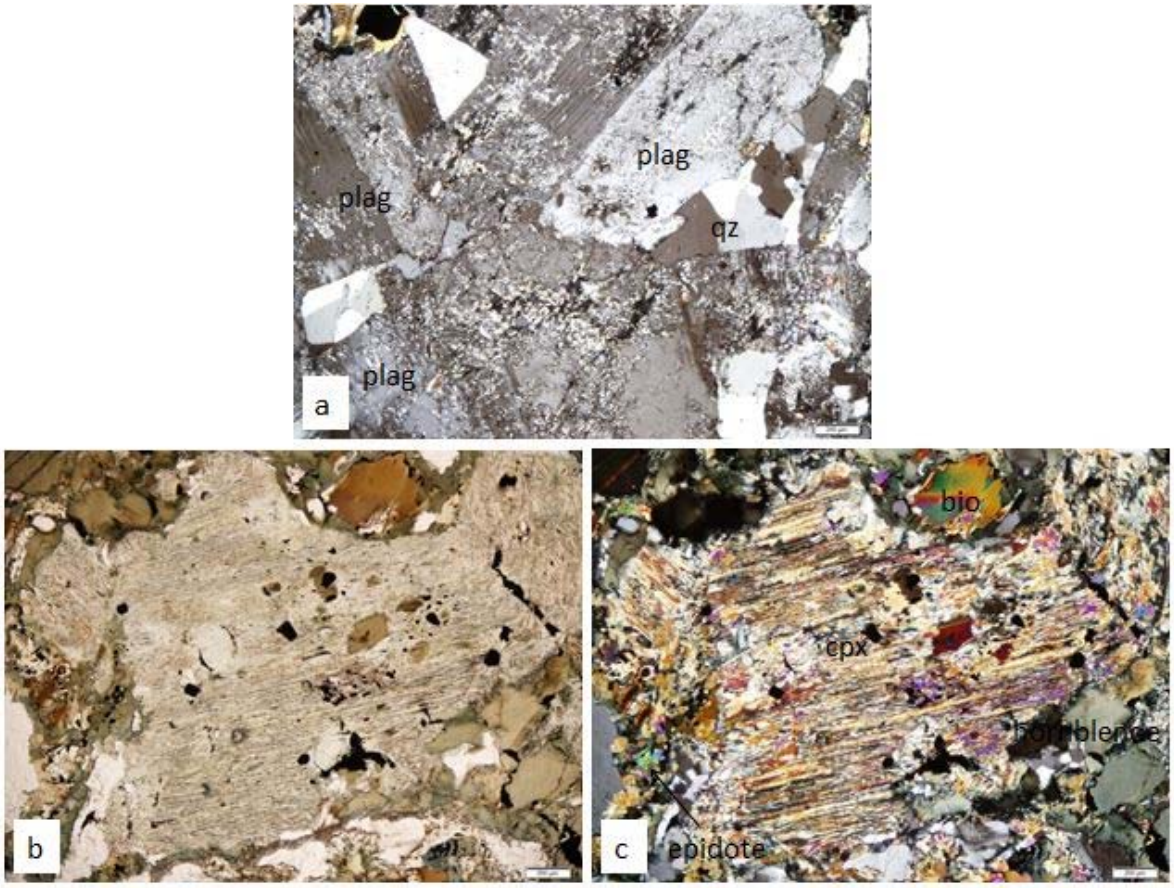

*Figure 16. Photomicrographs of the Gillstad gabbro thin section. Image **(a)** shows a coarse plagioclase grain with quartz in between (XPL), and **(b-c)** show an altered clinopyroxene with hornblende and biotite growing around and replacing the clinopyroxene (left PPL and right XPL). The scale bar in the lower right corner on all three images represents 200 microns.*

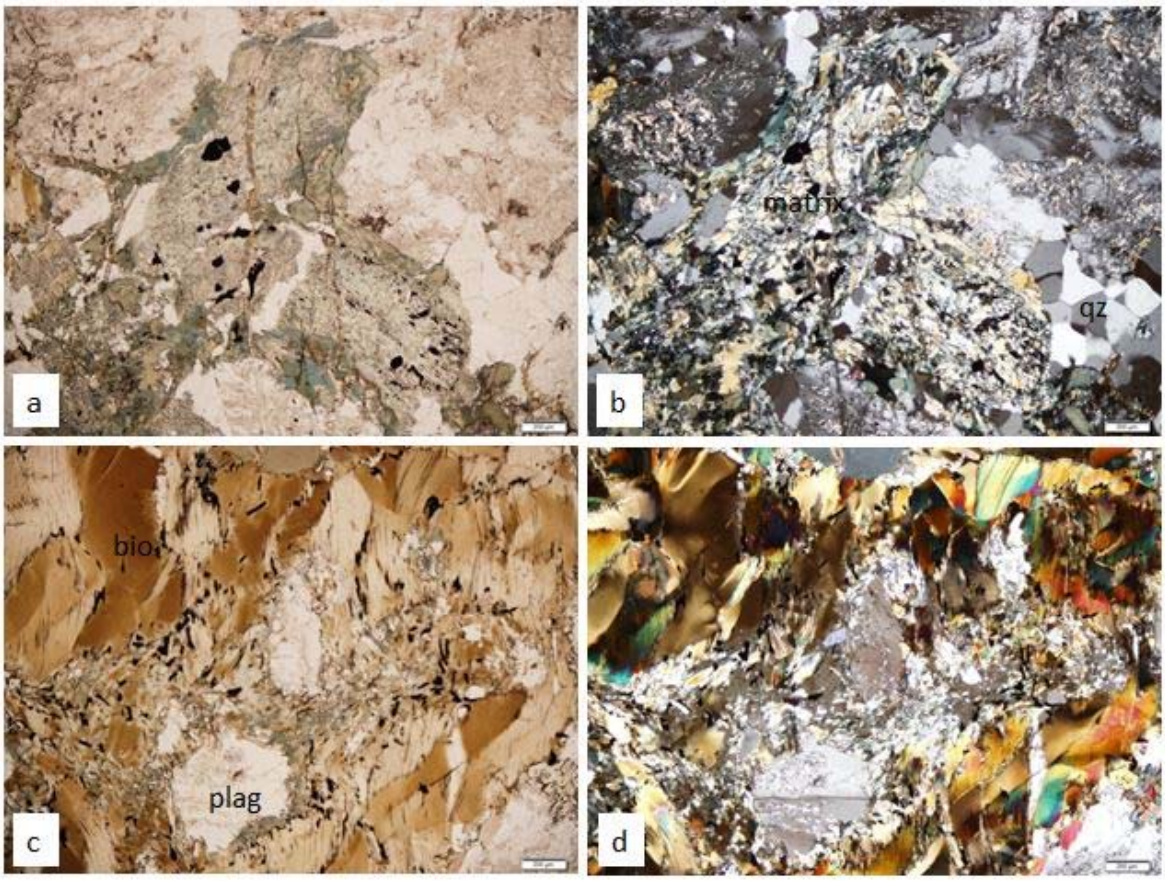

*Figure 17. Photomicrographs of the Gillstad gabbro thin section. Images **(a-b)** show the replacement pseudomorph of clinopyroxene, where matrix components are growing (left PPL and right XPL). Images **(c-d)** show slight foliation due to the growth of biotite approximately from north to south in the thin section (left is PPL and right is XPL). The scale bars in the lower right corner of all four images represent 200 microns.*

Flivik – granite

The Flivik granite hand sample is red to gray, inequigranular, medium to medium-coarse with larger feldspar grains. The main modal phases in the thin section are quartz, K-feldspar, plagioclase and biotite, with minor phases (approximately 1-2%) of magnetite, titanite (Figure 18 c-d) and accessory mineral phases (<1%) such as apatite, epidote and zircon (Table 12). The grain size is inequigranular ranging from coarse K-feldspars (microcline) and plagioclase grains to finer quartz. Quartz grain shapes are subhedral-anhedral, where grain size ranges from 3.5-0.3 mm (strained grains are larger) with mean size of 1.53 mm. Plagioclase grain shapes are subhedral-anhedral with grain sizes ranging from 4.5-0.8 mm (in longest dimension) with mean size of 1.84 mm, whereas K-feldspar (both microcline and orthoclase) grains are subhedral-anhedral and ranges from 1-9 mm (in longest dimension) with mean size of 2.92 mm. Biotite grains occur as flaky grains with subhedral-anhedral grain shapes. Quartz grains have both larger

strained grains and smaller grains that have tendencies to occur in interlocking clusters between grain boundaries of feldspar phenocrysts (Figure 18 b). Biotite also has a tendency of growing around feldspar phenocrysts which gives the impression that the grains are slightly folded. Feldspars have synthetic twinning textures where microcline can show both the characteristic tartan twinning as well as perthitic texture, and plagioclase shows albite twins. The even distribution of quartz and feldspar in the sample indicates that this sample can be classified as a monzogranite according to the QAP plot for igneous rock types (IUGS classification diagram, where QAP stands for quartz, alkali feldspar and plagioclase).

Table 12. Flivik granite specimen. Result of the point counting with major mineral phases and their respective volume fraction distribution.

Mineral phases	**Points counted**	**Volume fraction (%)**
Quartz	231	25
Plagioclase	188	24
K-feldspar	220	34
Biotite	99	13
Magnetite	17	2
Titanite	14	2
Totals	769	100

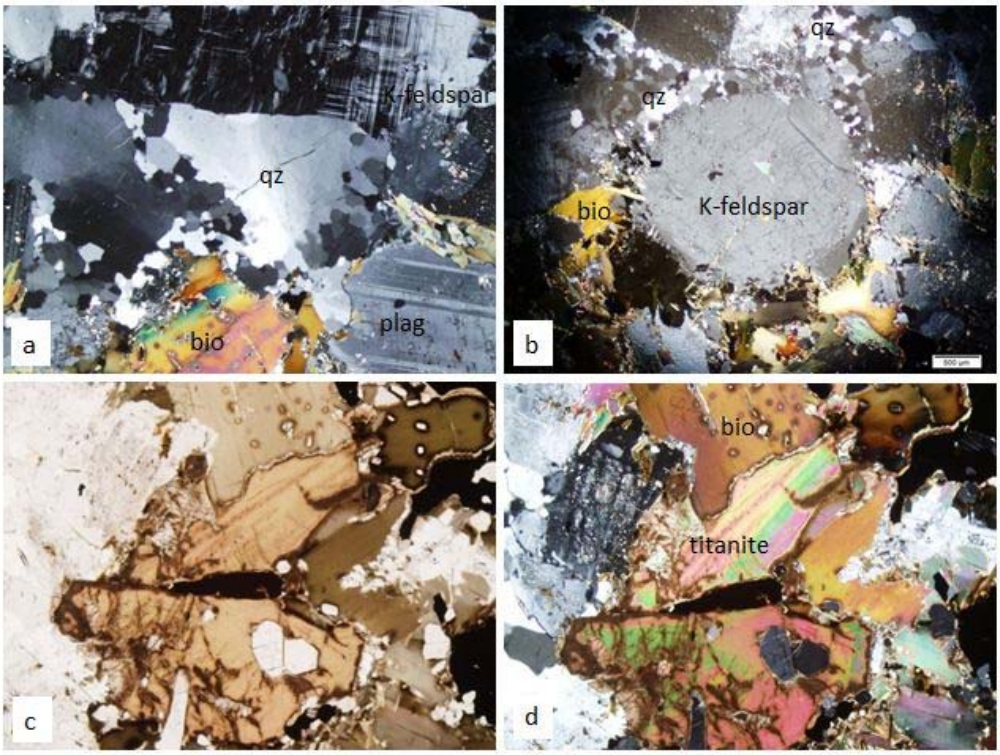

*Figure 18. Photomicrographs of the Flivik granite thin section. Images **(a-b)** demonstrate the overall mineralogy, where the quartz grows around the larger K-feldspar grain. The scale in the lower right corner is 500 microns in the right image (XPL) and 200 microns in the left image (XPL). Images **(c-d)** show titanite together with biotite and plagioclase in the thin section, where scale is represented as 200 microns (left PPL and right XPL)*

Fröland - granite with pegmatite

The granite is red, inequigranular, medium-grained and massive, with occasional pods of coarse-grained pegmatite. The hand sample is slightly weathered at the surface with possible alteration of feldspars to clay minerals and micas. The mineralogy of the thin section mainly consists of quartz, plagioclase and K-feldspar (microcline over orthoclase) with accessory minerals of muscovite, biotite and minor opaque phases (<1 %), such as magnetite (Table 13). Mineral grain size in the sample is inequigranular. Quartz has both strained and unstrained mineral grains with varying degree of undulose extinction. Quartz grain sizes ranges from 2.7-0.3 mm (where strained grains are larger) with mean size of 1.5 mm. Plagioclase grains sizes ranges from 3.5-0.6 mm (in longest dimension) with mean size of 1.73 mm whereas K-feldspar grains range from 4.5-0.3 mm (in longest dimension) with mean size of 1.38 mm. Plagioclase and K-feldspar (microcline) exhibit characteristic micro textures such as polysynthetic twinning, tartan twinning (Figure 19a-b) and perthitic intergrowths inside microcline. Replacement texture of muscovite (sericite) is evident in feldspar grains. Microcracks along with sericite occur mostly within mineral grains where quartz tends to have more cracks than feldspars (Figure 19b).

Table 13. Fröland granite specimen. Result of the point counting with major mineral phases and their respective volume fraction distribution.

Mineral phases	**Points counted**	**Volume fraction (%)**
Quartz	276	36
Plagioclase	235	31
K-feldspar	250	33
Totals	761	100

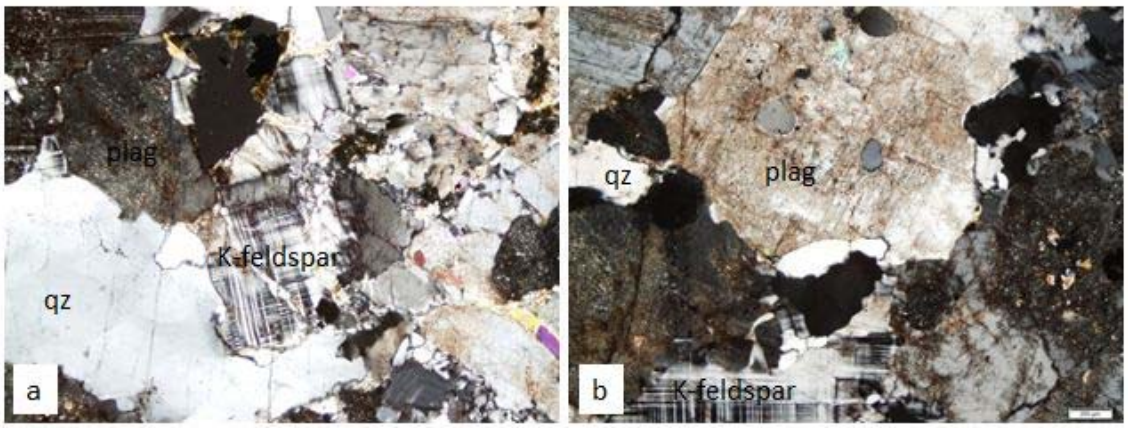

*Figure 19. Photomicrographs of the Fröland granite thin section. Images **(a-b)** demonstrate the overall mineralogy of the Fröland thin section, where quartz (strained and unstrained), K-feldspar (microcline) and plagioclase is present (left to right XPL). The scale bar in the lower right corner of the right image represents 200 microns, which is the same for the left image.*

Bårarp – granitic gneiss

The Bårarp granitic gneiss hand samples are gray to red, fine to medium grained, equigranular with a preferred grain orientation. The main mineralogy in thin sections A and B are K-feldspar (orthoclase over microcline), quartz, plagioclase and biotite with minor phases (1-3%) of amphibole (hornblende) and magnetite (Table 14). Accessory minerals in the samples (<1%) are zircon, apatite and epidote. A slight variation in composition is observed between the A and B samples; A has a greater fraction of quartz with less feldspars and B has higher fractions of feldspars and amphiboles. Minerals grains in A and B are equigranular with granoblastic texture and with straight grain boundaries (Figure 20a-c) in both samples. Quartz grains are subhedral-anhedral and range from 1-0.1 mm, with mean size of 0.5 mm and can appear both as stained and unstrained. Plagioclase grains are subhedral-anhedral and range from 1-0.3 mm with mean size of 0.6 mm, where K-feldspar are subhedral-anhedral and range from 0.4-0.1 mm with mean size of 0.35 mm. Biotite grains are elongated subhedral-euhedral with grain size ranging from 0.5-0.1 mm. Hornblende grains are subhedral with grain size ranging from 0.3-0.1 mm. The samples display foliation texture due to the alignment of micas and amphiboles across the entire sample

(Figure 20a-c). Feldspars have common textures of polysynthetic twins and tartan twinning. Seritization of feldspars (mainly plagioclase) occurs in lesser extent within microcracks and between grain boundaries. Another alteration texture observed in the sample is occasional chloritization of biotite and amphiboles, although not a very common one.

Table 14. Bårarp gneiss A & B specimen. Result of the point counting with major mineral phases and their respective volume fraction distribution.

Mineral phases	Points counted (A)	Volume fraction (%)	Points counted (B)	Volume fraction (%)
Quartz	233	29	210	26
Plagioclase	216	27	234	29
K-feldspar	252	31	262	32
Biotite	72	9	71	9
Hornblende	14	2	25	3
Magnetite	14	2	12	1
Totals	801	100	814	100

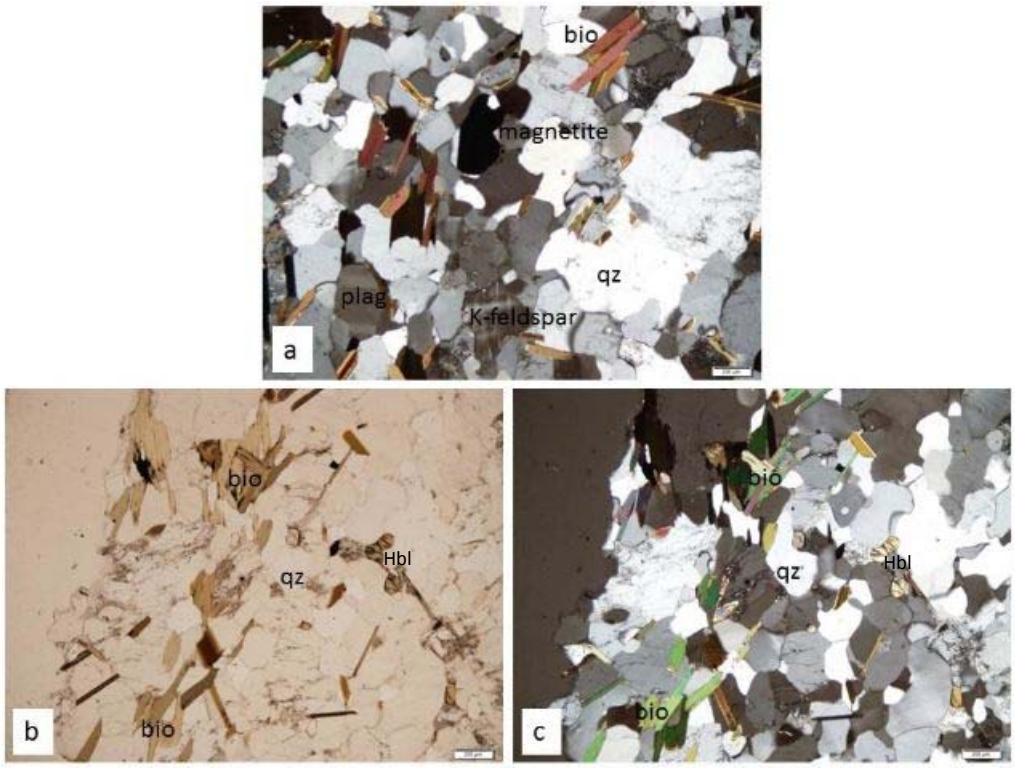

*Figure 20. Photomicrographs of the Bårarp granitic gneiss thin sections. Images **(a-c)** show the overall mineralogy of the Bårarp thin sections, where quartz, plagioclase, K-feldspar (mostly orthoclase, but also microcline), biotite and hornblende are present (**a** and **c** is XPL, while **b** is*

PPL). Notice that the foliation direction in the images. The scale bar in the lower right corner of each image is represented by 200 microns.

6.3 Theoretical calculation of thermal conductivity and heat capacity

The calculated thermal properties (thermal conductivity and volumetric heat capacity) of the seven specimen are summarized in Table 15.

Table. 15. Thermal conductivity and volumetric heat capacity results from calculation. For more information about the procedure of calculation, see Appendix 1-3.

Specimen	Forserum quartzite	Forserum diabase	Gillstad	Flivik	Fröland	Bårarp A	Bårarp B
λ (W/mK) calculated	4.24	2.08	2.41	3.61	4.17	3.82	3.6
Cv (MJ/m^{3}K) calculated	1.48	2.11	2.06	1.86	1.81	1.88	1.88

7. Discussion

Mineralogical and petrographic impacts on thermal properties

The seven different specimens were chosen to test if mineralogy affects thermal conductivity and heat capacity based on varied modal composition and mineralogical associations (felsic to mafic). In order to put the mineralogical information into perspective, the similarities of the major mineral phases in the granitic and the mafic specimens together with the quartzite (now called skarn) have be compared. The granitic specimens (Flivik, Fröland and Bårarp A & B) consists of 25-35% quartz and feldspar (including plagioclase and K-feldspars) with additional biotite (up to 9%). The mafic specimens (Forserum diabase and Gillstad gabbro) have 55-65% plagioclase, 4-22% clinopyroxenes, 13% biotite and about 10% hornblende. The measured values of thermal conductivity (Figure 9) show that the granites (Fröland and Flivik) and the skarn have the highest value (3.82-3.05 W/mk), while the diabase has the lowest value (2.46 W/mk) followed by the gabbro (2.61 W/mk). The main mineralogical and most normal difference in these specimens is the content of the quartz phase, regardless of felsic or mafic composition. Birch & Clark (1940) argued that the molecular movement (vibration) through the silicon-oxygen tetrahedral structure in most silicates is the dominating factor that affects thermal conductivity overall.

The reasonable theory of Birch & Clark (1940) does however not apply to all measured specimens. The Bårarp granitic gneiss specimens have similar modal composition compared to the other granitic specimens with high quartz content (26-29%), but display low measured values of thermal conductivity. This clearly contradicts the previous statement as the difference is about 35% when comparing the Fröland and Bårarp A sample (see Figure 9), where the Bårarp A has almost the same value as the diabase. The main difference between the specimens is that the Bårarp gneiss is metamorphic and foliated. The Bårarp specimens could therefore be compared with the metamorphosed Forserum skarn. This specimen consists of approximately the same quartz content (26%, matrix proportion included), 45% calcite (matrix included) and 14%

plagioclase. These two specimens differ by 26% in measured thermal conductivity although having similar quartz values. Thus, it becomes apparent that petrographic parameters other than mineralogy also affect the measured thermal conductivity.

The calculated values for thermal conductivity shows a similar response to the measured values, where felsic samples always have high thermal conductivity over mafic. When comparing the calculated values of the Fröland granite (4.17 W/mK) to the Forserum diabase (2.08 W/mK), it becomes clear that the response is two times higher if the calculated situation is compared. As the main difference between the specimens is the quartz content, this must also affect the outcome of calculated values. This notation is valid when observing the literature values from Horai (1971) in Table 5, which indicate that quartz has almost four times higher conductivity compared to feldspars and biotite, three times higher than hornblende and two times higher than augite.

When correlating the high conductive SiO_2-phase with the thermal conductivities of the measured and calculated values (Figure 21), a difference between the two datasets arises; the calculated conductivities have a much stronger correlation coefficient (R^2=0.93) than the measured conductivities. The result is probably related to the high conductive value of quartz in the literature data, the observed fraction of quartz in the specimens and the arrangement of Equation 6. The correlation coefficients of the measured values also appear significantly lower due to the TPS not taking specific mineralogical phases into account, which would also explain the overestimation of thermal conductivity in the calculated values.

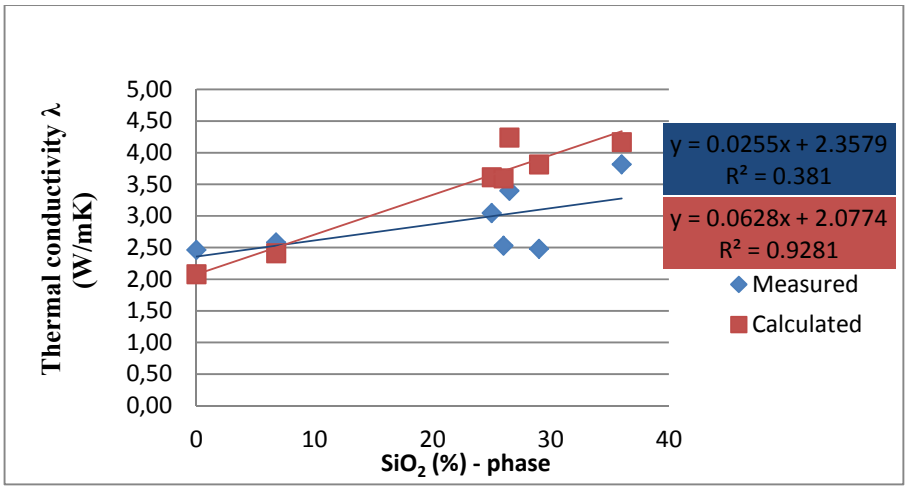

Figure 21. The correlation of the quartz content in the specimens with the measured and calculated thermal conductivity.

Heat capacity on the other hand shows less variance with mineralogy compared to thermal conductivity (Table 5-6). This can also be observed in measured values in Table 7 and Figure 9, where the values between the highest (diabase) and lowest (Bårarp A) differ by 25%. The traditional explanation is that minerals with higher density have higher heat capacity compared to lower density (i.e. mafic minerals to felsic association), (Kukkonen & Lindberg, 1998 and

Cermak & Rybach, 1988). This is only partly true when observing the measured values in Table 7, where the Fröland specimen has higher heat capacity than the mafic gabbro. As heat capacity is not directly measured with the TPS, this is probably both a direct and indirect response of mineralogy. Quartz has been reviewed by Höfner & Schilling (2002) to be a major mineral with the greatest influence on thermal diffusivity in crystalline rocks, which would also explain the overall high values in the Flivik and Fröland specimen in the measured TPS values. This makes it hard to establish a general relationship of mineralogy in terms of mineral association from mafic to felsic based on the TPS values. The calculated values on the other hand show a clearer relationship, where the mafic specimen have the highest value for volumetric heat capacity over the granitic specimen. A problem that arises with the utilization of literature values for heat capacity is where no specific value for a desired mineral is declared, which was the case in the skarn (andradite) and the Flivik granite (titanite).

As mentioned earlier in the discussion, the quartz content may not always be the driving parameter for thermal conductivity (the Bårarp example). The other main difference between the specimens is the grain size. Mineral grain size was therefore analyzed in five of the seven thin sections, where the Bårarp A was not analyzed due to having the same grain size as Bårarp B, and the skarn having too complex and varied grain size. As thermal conductivity can be seen as the vibration of atoms through a crystal lattice, it would be more efficient to move through the same crystal rather than moving through different crystals with different properties (arguably the case in polycrystalline materials). A good example of varied grain sizes can be observed in the granitic specimen where the normal assumption would range the Bårarp granitic gneiss as the specimen with smallest and the Fröland pegmatite granite as the specimen with largest grain size. These specimens also have very similar mineralogy (quartz, K-feldspar and plagioclase), which makes them a good comparison to investigate if larger grain size has any relationship with thermal conductivity or possibly with heat capacity. The same comparison could be applied to the mafic specimen (plagioclase, clinopyroxenes).

Thirty grains of quartz, plagioclase and K-felspar were therefore randomly measured in the longest direction (90 points in total) in each of the three granitic thin sections (Bårarp, Flivik and Fröland), and plagioclase and augite was measured in the mafic specimens (diabase and gabbro). Due to varying grain sizes in the Fröland, and especially the Flivik thin section, compared to the Bårarp thin section, an average grain size was calculated for all individual specimens. The same procedure was performed for the mafic samples (see Appendix 4-8). The average grain size was plotted with both the measured and calculated thermal conductivity in Figure 22-23, as well as with the volumetric heat capacity in Figure 24-25, to determine their relationship. It becomes apparent by observing Figure 22-23 that thermal conductivity does not increase with larger grains size in either the granitic or mafic association. The Flivik specimen had the greatest measured average grain size among the granitic samples but did not correspond with the highest thermal conductivity, with no linear relationship. The mafic samples demonstrated only slightly different average grain size (approximately 0.2 mm) but did not show a linear relationship by increasing

grain size. However, Ramakrishnan et al., (2012) claims that an increasing average grain size has a strong correlation (R^2=0.97 with a second order polynomial fit) with increasing thermal conduction. This would either mean that there is a relationship, or that the approach of using average grain size as a representative method is inappropriate to determine such a relationship. Heat capacity showed a relationship of average grain size compared to both measured and calculated heat capacity in the mafic specimens, where the Forserum diabase yielded the highest value (Figure 24-25). Although presented as a result, it is questionable if the diabase specimen actually has larger average grain size than the gabbro when investigating the thin section by the unaided eye. It is more likely that the density of minerals have greater impact on heat capacity than grain size. Grain size is therefore interpreted to not affect heat capacity.

Although grain size not directly affect the thermal conductivity, this can indirectly cause problems to thermal conductivity in a specimen when considering the resulting grain boundaries of different grain sizes. The granitic samples displayed varying grain sizes and different textures when comparing the coarser inequigranular Flivik and the Fröland granites with the finer grained granoblastic Bårarp specimens and thin sections. As the Bårarp gneiss samples have smaller grain size this will ultimately result in more grain boundaries than the coarser granites which is probably reflected in the direct TPS values. The concept can also be applied to the mafic specimens, where the average grain size of the plagioclase and clinopyroxenes are similar for both thin sections, and that they displayed coarse textures.

There have been several attempts to theoretically model thermal conductivity in nanocrystalline material (mostly graphene or diamonds) according to grain size (Dong et al., 2014). The authors claim that smaller grain size will generate more obstacles (i.e. grain boundaries) which will increase the thermal resistance for the vibrations between the mineral interfaces. Inversely, an increasing grain size will decrease the scattering of vibration as fewer grain boundaries will appear. Birch & Clark (1940) also emphasized that thermal resistance is an important thermo-physical aspect of thermal conduction in polycrystalline rocks. Although no direct attempt was performed to analyze or quantify the effect of grain boundaries and thermal resistance in the thin sections, the theoretical concept of thermal resistance at grain boundaries could be applied to some extent in this report.

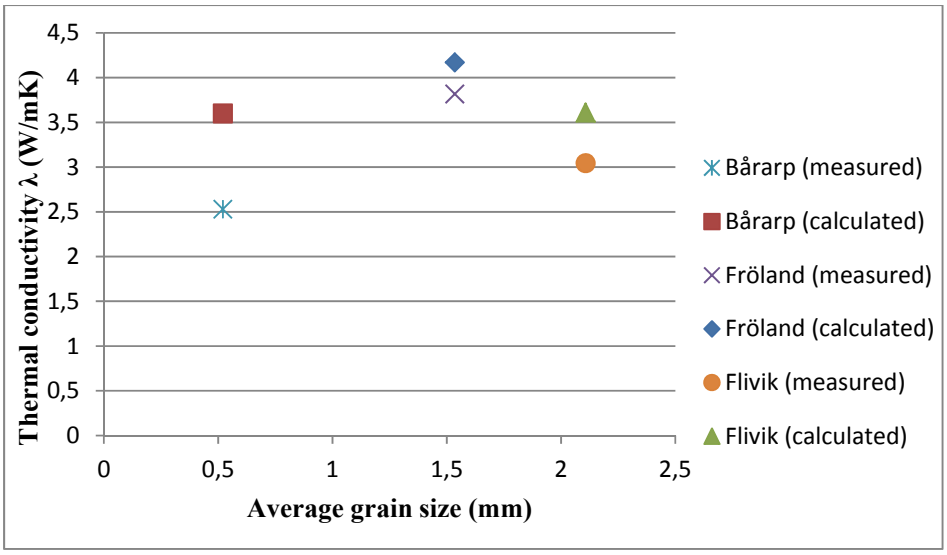

Figure 22. The measured average grain size of the granitic specimen in relation to the measured and calculated thermal conductivity. No correlation is shown in the graph due to few data points for a representative correlation.

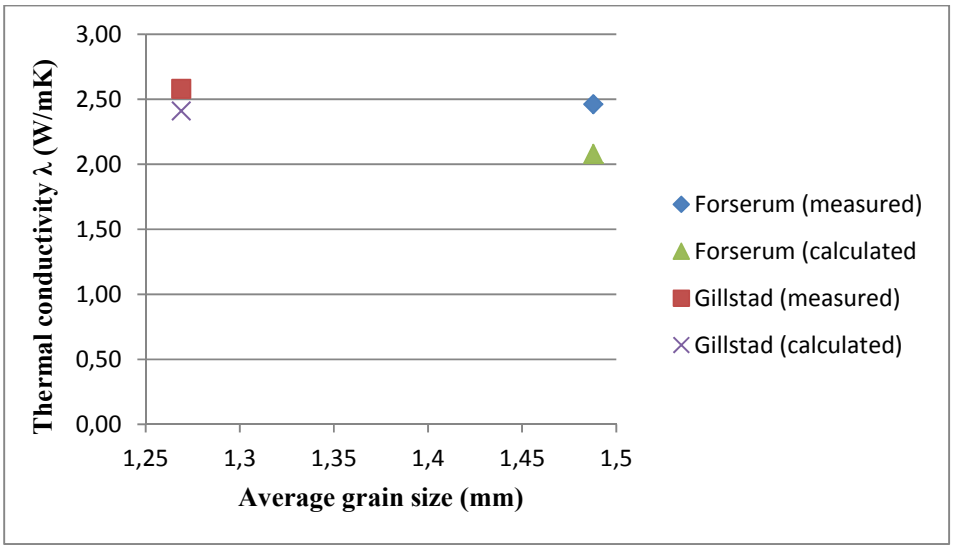

Figure 23. The measured average grain size of the mafic specimen in relation to the measured and calculated thermal conductivity. No correlation is shown in the graph due to few data points for a representative correlation.

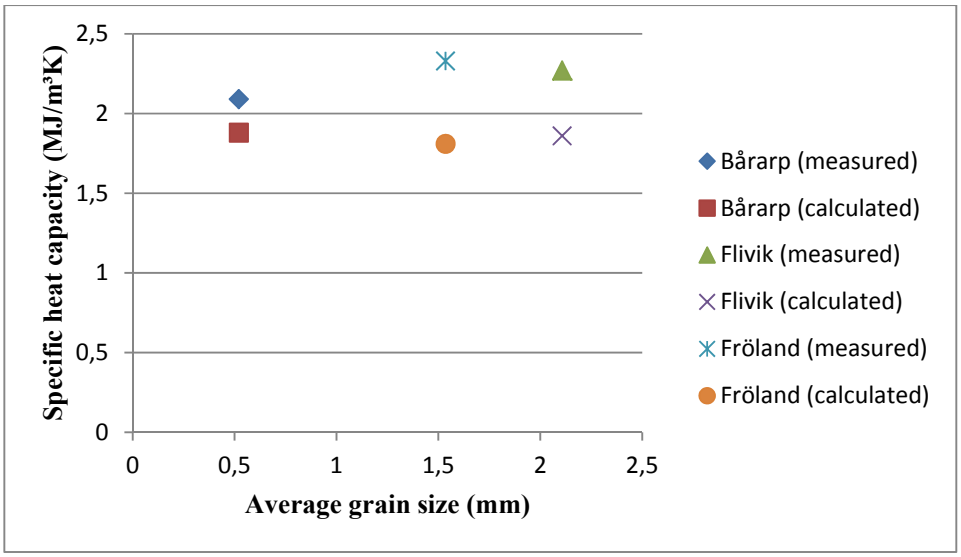

Figure 24. The measured average grain size of the granitic specimen in relation to the measured and calculated thermal volumetric heat capacity. No correlation is shown in the graph due to few data points for a representative correlation.

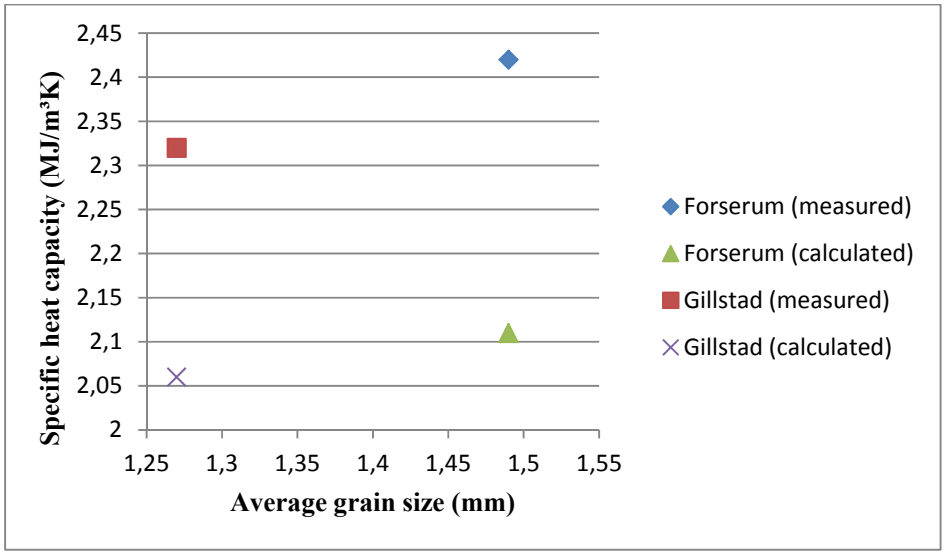

Figure 25. The measured average grain size of the mafic specimen in relation to the measured and calculated thermal volumetric heat capacity. No correlation is shown in the graph due to few data points for a representative correlation.

The Bårarp granitc gneiss samples (A & B) are foliated and were therefore divided into two specimens and thin sections, due to the possibility of acquiring information about anisotropy by measuring conductivity in the opposite directions of the foliation. Gneisses and granitic gneisses are generally reviewed to have a wide range of values due to anisotropy and measurement in different foliation directions (Schön, 2011, Clauser & Heugenes, 1995, Sundberg, 2009, Adl-

Zarrabi et al., 2008). The two Bårarp specimens have very similar conductive properties, although foliation was in opposite directions during measurements, where the anisotropy between the samples thermal conductivity was approximately two percent according to the TPS-measurements (λA/λB). The anisotropy in the specimens are apparently not enough to generate great differences in conductivity and can therefore not be seen as a factor in this case. It is possible that foliation together with the microstructure (grain boundaries indirectly with small grain size) might be the reason why the specimens have so low thermal conductivity.

Further aspects that might be relevant mentioning from the petrographic analysis are the formation of secondary crack alteration in the Forserum diabase and replacement textures. The Forserum diabase block did not show any sign of alterations at the point of sample collection, but was, after cutting, recognized to have alteration cracks with secondary minerals. These cracks exhibited cataclasitic textures which points to mechanical deformation with a later recrystallization of K-feldspar (probably adularia under the circumstances) as groundmass in the cracks according to SEM analysis. These small-scale cracks run along the entire thin section and would probably interfere with the conductivity as the drastic change in the crystal would probably cause a decrease in the general conductivity for the sample, according to the theory of thermal resistance. It is also observed that the diabase has slightly lower conductivity than the gabbro. The crack matrix was approximated to only four percent in the diabase thin section, which makes it difficult to estimate the exact extent of this aspect in contrast to mineralogical influence with only petrographic analysis. The same example could be applied to the extensive replacement textures in the gabbro sample, where clinpyroxenes are altered to a point where a concept thermal property for a uniform phase becomes unclear. The matrix present in the gabbro and diabase specimens may also be affected by the previously mentioned thermal resistance, as it creates more grain boundaries. Applying the concept of thermal resistance to the Forserum skarn may explain the anomalous thermal conductivity apart from modal composition. It is however reasonable to think that alteration, matrix and cracks would have a lesser effect on heat capacity as it does not involve the same process as conduction. Furthermore, the diabase is the only specimen that has developed cracks but is at the same time the specimen with the highest heat capacity, so this is obviously not the case. Another example could be the relatively altered gabbro, which apparently does not cause it to decrease in heat capacity compared to the other specimens. It could thereby be argued that heat capacity is not affect by such features.

Petrographic analysis vs Hot Disk TPS

The comparison between the Hot Disk TPS measured thermal conductivity and the calculated thermal conductivity from tabulated values and obtained volume fractions is summarized in Table 16. The correlation between the measured and calculated values (Figure 26) yielded a positive but moderate correlation (R^2=0.44). This is not a surprising result when considering the differences between the measured and calculated values range from 7-35%. The most deviating specimens are the Bårarp granitic gneiss specimens, which clearly are not represented by the parallel equation (6). This is probably due to the overestimation in the equation when using

theoretical values of high conductive quartz (as discussed previously in the discussion) and the fact that anisotropy together with other petrographic parameters are not included in the equation. Sundberg et al. (1985) addressed a similar flaw in the geometric equation (which is slightly different from Equation 6), with no specific orientation of mineral grain or grain shapes. They proposed a correction of phases with high thermal conductivity (i.e. quartz) in rock types, but later stated that this correction only has an arbitrary relation as the phase already is included in the original equation. The calculated values for the mafic specimens resulted in lower values than the measured values of the TPS, which is the opposite of the granitic specimens. The TPS measurements are according to the measurements (Appendix 9-15) very accurate, which means that the prediction in either the parallel equation, the values from Horai (1971) or misinterpretation of the modal analysis is the main source of error. Misinterpretation of the modal analysis through point counting did occur at several instances and specifically in the skarn and gabbro samples. A problem with the literature values is the methodology Horai (1971) used for acquiring the data set. Horai measured thermal conductivity on pulverized aggregates with known monomineralic composition which is an ideal situation compared to the polycrystalline situation in actual rocks (see section 4.6.4). A direct error with literature values is also that all desired minerals have not been listed in literature, which means that this approach cannot be used on all rock types (although most common rock types can be theoretically calculated.) Several authors (Baldridge & Horai 1972, Sundberg et al. 1985) have however calculated thermal conductivity with satisfying results with similar equations, so this cannot be entirely ruled out. It can be argued that the Bårarp specimens have such a large impact on the equation that these values become less credible due to the direct involvement of these. When all the values beside the gneiss specimens were plotted together, a better correlation occurred (R^2=0.88), which would indicate that the measured values are in good agreement without the Bårarp specimen (Figure 27). Calculating thermal conductivity as a method could still be sufficient as an economical alternative in some cases compared with the TPS-measurements (based on the previously mentioned correlation), but cannot be proved in this specific study as a statistical certainty based on the presented values.

The comparison between the measured and calculated volumetric heat capacity showed very low correlation according to Figure 28. This is probably due to the fact that the literature values are very close in the range (Table 17), as argued earlier in the discussion. Problems with the calculations are also based on the same principles as for thermal conductivity (modal analysis, literature data) and the fact that heat capacity is measured indirectly. As the values do not deviate much between measured and calculated values (compared to thermal conductivity values), it is difficult to say if the correlation is sufficient for this method to be used as an alternative to direct measurements.

Table 16. The results from the measured (Hot Disk TPS) thermal conductivity values and calculated thermal conductivity values from Equation 6 with their respective differences.

Specimen	Skarn	Diabase	Gillstad	Flivik	Fröland	Bårarp A	Bårarp B
λ (W/mK) measured	3.40	2.46	2.58	3.05	3.82	2.48	2.53
λ (W/mK) calculated	4.24	2.08	2.41	3.61	4.17	3.82	3.60
Difference (%)	20	15	7	15	9	35	30

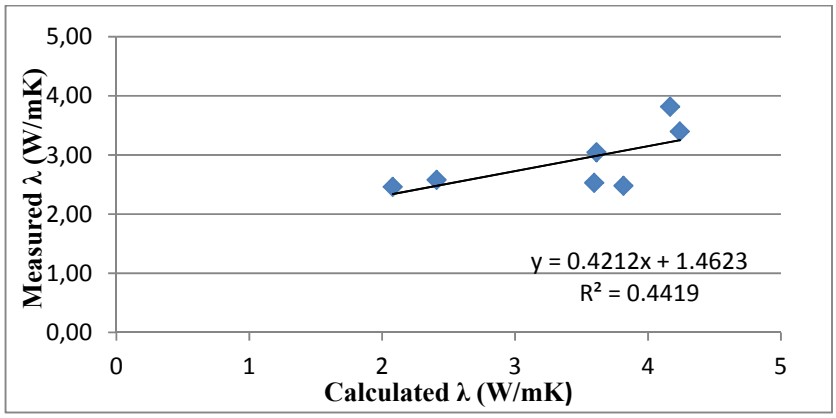

Figure 26. The graph shows the correlation between the two data sets in Table 16, where the R^2 of 1 would demonstrate a perfect correlation coefficient. The correlation was not set to intercept at origo which gives a floating line of a best fit.

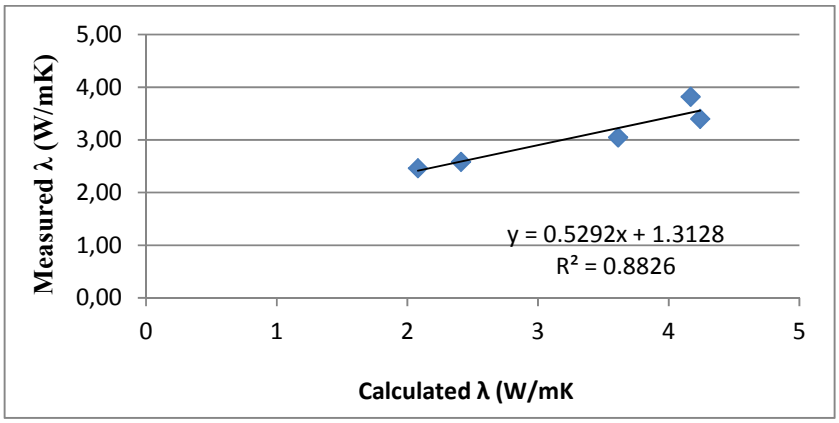

Figure 27. The graph shows the correlation between the two data sets in Table 16 excluding the Bårarp samples (notice that the correlation coefficient changes from Figure 26 after excluding the two samples). The correlation was not set to intercept at origo which gives a floating line of a best fit.

Table 17. The results from the measured (Hot Disk TPS) volumetric values and calculated volumetric heat capacity with their respective differences.

Specimen	Skarn	Diabase	Gillstad	Flivik	Fröland	Bårarp A	Bårarp B
Cv (MJ/m^{3}K) measured	2.26	2.42	2.32	2.27	2.33	1.83	2.09
Cv (MJ/m^{3}K) calculated	1.48	2.11	2.06	1.86	1.81	1.88	1.88
Difference (%)	35	13	12	19	22	3	10

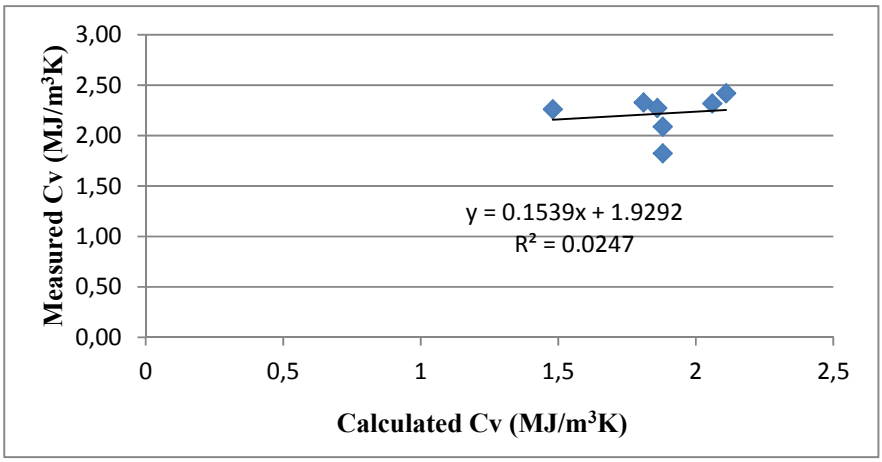

Figure 28. The correlation between the volumetric heat capacity obtained from TPS measurement and the calculated volumetric heat capacity.

It is important to understand that the mathematical approaches have limitations as they are built on a perfect assumption that complex polycrystalline material are perfectly distributed after modal analysis with little influence of other petrographic parameters. The calculated thermal conductivity used in this article is based on values of monomineralic composition and does not entirely explain complex situations. The conditions needed for an economical and environmental usage of Equation 6 instead of direct measurement on crystalline rocks arises when:

- samples and thin sections are representative and straightforward
- modal data is cheap to obtain
- the person performing modal analysis has sufficient skills in petrography
- thermal conductivity data for all present mineral phases can be found in the literature

Further suggested investigations would be to study the influence of grain boundaries in crystalline rock material with varying grain sizes. It should be added that direct measurements may be a necessary compliment when investigating the thermal properties of a rock.

8. Conclusions

- Thermal conductivity of the specimens can be considered to have a correlation with existing modal composition, where felsic mineralogy with high quartz content (Fröland 3.82 W/mK and Flivik 3.05 W/mk) has a clear tendency of having higher thermal conductivity over mafic mineralogy, and low quartz content (Forserum 2.46 W/mk and Gillstad 2.58 W/mk). Mineralogical content seems to correlate with calculated volumetrical heat capacity to some extent, but has no clear relationship when comparing the measured typical felsic (Fröland at 2.33 MJ/m³K) and mafic (Forserum diabase at 2.42 MJ/m³K) specimens.

- Mineral grain sizes per se do not show a strong relationship with thermal conductivity or volumetric heat capacity, although indirect microstructure of grain size (i.e. grain boundaries) might have an impact due to thermal resistance for thermal conductivity. Other petrographic features that might affect thermal conductivity are the alteration in the Gillstad gabbro, the cataclasititc cracks in the Forserum diabase and the matrix in the Gillstad and skarn samples. Foliation is not a feature that created great anisotropy of thermal conductivity across the different mineralogical orientation in the gneiss specimens. Alteration and cracks in the samples is argued to have less implication on volumetric heat capacity of the specimens.

- Petrographic analysis together with the parallel equation yield reasonable correlation (R^2=0.88) without the Bårarp gneiss specimens, but yield a moderate correlation when included (R^2=0.44). This correlation could indicate that this method might work as an alternative for predicting thermal conductivity over the direct Hot Disk TPS instrument, but has certain limitations. This method could also be used from an economical and environmental standpoint if certain requirements are fulfilled. It is also required that the person investigating the modal data have extensive knowledge about petrography to accurately estimate a representative modal composition. Direct measurements will therefore be a necessary compliment to provide an accurate representation of rock's thermal properties in future studies.

9. References

Adl-Zarrabi, B., Christianson, R., Sundberg, J., & Wrafter, J. (2009). *Measuring anisotropic thermal properties of metagranite at different scales*. SKB.

Anolfsson, T. (2013). *Analyses of thermal conductivityfrom mineral composition and analyses by use of Thermal Conductivity Scanner: A study of thermal properties in Scanian rock types*. University of Lund, department of geology.

Best, M. G. (2003). *Igneous and metamorphic petrology*. Second edition. Blackwell science ltd. P 2-7, 52-55.

Birch, F., & Clark, H. (1940a). *The thermal conductivity of rocks and its dependence upon temperature and composition, Part I*. Am. J. Sci., 238(8), 529-558.

Birch, F., & Clark, H. (1940b). *The thermal conductivity of rocks and its dependence upon temperature and composition, Part II*. Am. J. Sci., 238(9), p 613-635.

Cermak, V., & Rybach, L. (1982). *Thermal conductivity and specific heat of minerals and rocks, in Landolt-Bornstein: Numerical Data and Functional Relationships in Science and Technology*. Geophysics and Space Research: Physical Properties of Rocks, Volume la, p 305-343.

Çengel, Y. A., & Boles, M. A. (2006). *Thermodynamics - An engineering approach*. Fifth edition. McGraw-Hill Education, p 51-55, 60, 70-73, 92.

Chan, J. (2013). *Thermal properties of concrete with different Swedish aggregate materials*. University of Lund.

Clauser, C., & Huenges, E. (1995). *Thermal conductivity of rocks and minerals, in: Rock Physics and Phase Relations_A Handbook of Physical Constants*. AGU.

Clark, S. (1966*). Handbook of Physical Constants, Memoir 97*. New York: Geological Society of America.

Dong, H., Wen, B., & Melnik, R. (2014). *Relative importance of grain boundaries and size effects in thermal conductivity of nanocrystalline materials*. Scientific reports, 4:7073.

Eliasson, T., & Schoberg, H. (1991). *U-Pb dating of the post- kinematic Sveconorwegian Bohus granite. SW Sweden: Evidence of restitic zircon*. Precambrian Research 51.p 337-350.

Faure, G. (1998). *Principles and application of geochemistry*. Second edition. Prentice Hall, New Jersey.

Gustafsson, S. E. (1991). *Transient plane source techniques for thermal conductivity and thermal diffusivity measurements of solid materials.* AIP publishing. Review of Scientific Instruments, 62.

Hashin, Z., & Shtrikman, S. (1962). *A variational approach to the theory of the effective magnetic permeability of multiphase materials*. J. Appl. Phys. 33, 3125.
Herzen, V. R., & Maxwell, A. E. (1959). *The measurement of thermal conductivity of deep-sea sediments by a needle probe method*. J. Geophys. Res. 64.

Horai, K., & Simmons, G. (1969). *Thermal conductivity of rock-forming minerals*. Earth and Planet. Scences. Letters v 6, 359-368.

Horai, K. I. (1971). *Thermal conductivity of rock-forming minerals*. J. Geophys. Res. 76 (5), 1278-1308.

Horai, K., & Baldridge, S. (1972a). *Thermal conductivity of nineteen igneous rocks, I Application of the needle probe method to the measurement of the thermal conductivity of rocks.* Phys. Earth Planet. Interiors (5) 151.

Horai, K., & Baldridge, S. (1972b). *Thermal conductivity of nineteen igneous rocks, II Estimation of the thermal conductivity of rock from the mineral and chemical compositions*. Phys. Earth Planet. Interiors (5) 157.

Höfer, M., & Schilling, F. R. (2002). *Heat transfer in quartz, orthoclase and sanidine at elevated temperature*. Physics and Chemistry of Minerals, 29, 571–584

Kapitza, P. L. (1941). *The study of heat transfer in helium II.* J. Phys. USSR 4, 181.

Kukkonen, I., & Lindberg, A. (1998). *Thermal properties of rocks at the investigation sites: measured and calculated thermal conductivity, specific heat capacity and thermal diffusivity*. Posiva OY, Helsinki. Geologic Survey Finland, 98-09e.

Lundqvist, J., Lundqvist, T., Lindström, M., Calner, M., & Sivhed, U. (2011). *Sveriges geologi from urtid till nutid.* Tredje upplagan. Studentlitteratur AB, Lund. P 169-178.

Melnikov, N. W., Rshewski, W. W., & Prodotjakonov, M. M. (1975). *Sprav. ocnik (kadastr.) Fiziceskich Svoistv Gormich Porod.* Izdat Nedra, Moskva.

Möller, C., Andersson, J., Lundqvist, I., & Hellström, F. (2007). *Linking deformation, migmatite formation and zircon U-Pb geochronology in polymetamorphic orthogneisses, Sveconorwegian Province, Sweden. Journal of metamorphic Geology,25, p 727-750.*

Ramakrishnan, D., Bharti, R., Nithya, M., Kusuma, K. N., & Singh, K. D. (2012). Measurement of thermal properties of select intact and weathered granulites and their relationship to rock properties. *Geophysics, 77*(3), D63-D73.

Scherstén, A. (2002). *187Re- 187Os evidence for crustal lenses of Svecofennian age within the Mylonite Zone*. SW Sweden. *GFF*, p 35-39.

Schön, J. H. (2011). *Physical properties of Rocks: A Workbook.* Volume 8. Great Britain: Elsevier. P 337-372.

Sundberg, J., Thunholm, B., & Johnson, J. (1985). *Värmeöverförande egenskaper i svensk berggrund*. Statens råd för byggforskning, Stockholm. Liber Tryck AB.

Sundberg, J. (1991). *Termiska egenskaper i berg och jord*. Tryck-Center, Linköping. SGI.

Sundberg, J., Back, P. J., Ericsson, L. O., & Wrafter, J. (2009). *Estimation of thermal conductivity and its spatial variability in igneous rocks from direct density logging*. Elsevier.

Söderlund, U., Patchett, P. J., Vertoort, J. D., & Isachsen, C. E. (2004). *The ^{176}Lu decay constant determined by Lu-Hf and U-Pb isotope systematics of Precambrian mafic intrusions*. Earth and Planetary science letters, Volume 219 pages 311-324.

Electronic sources

http://www.hotdiskinstruments.com (2015-05-29)

http://www.minoprep.se/ (2015-05-29)

http://webmineral.com/ (2015-05-29)

10. Acknowledgements

I would like to post a word of gratitude towards my supervisor Linus Brander at CBI who supported, encouraged and guided me throughout the thesis. Special thanks dedicated to employees Johan Sjöström and Bengt Bogren at SP Fire Research for performing the Hot Disk TPS measurements and for lending helpful expertise. Thanks to Johan Hogmalm and Mark Johnson for being my supervisor and examiner at Geovetarcentrum. Thanks to Johan Gunnarsson-Wikholm for critical reading and especially to Emelie Wetterling for her steady support and thorough proofreading. Last but not least a thanks to Swerock, Skanska, Emmaboda granit AB who provided the material.

11. Appendices

Appendix 1-2. Left to right shows the conversion from specific heat capacity to volumetric heat capacity. The procedure is performed by utilizing literature values from Melinkov et al (1975) and Cermak & Rybach (1982) which have to be converted from specific heat capacity into volumetric heat capacity. This was done to compare the measured heat capacity with the calculated. The literature values are made into an average specific heat capacity for each mineral which is multiplied with the specific gravity of each mineral (retrieved from mineraldata.com) to obtain the right unit for volumetric heat capacity. The results are finally divided by 1000 to obtain MJ/m^3 K. The calculated values for volumetric heat capacity for all specimens can be observed below.

Mineral phases	Melnikov et al. (1975)	Cermak & Rybach (1982)	Average	Density (kg/m^3)	Cv (kJ/m^3 K)	Cv (MJ/m^3 K)
Quartz	0.74	0.7	0.72	2650	1908	1.908
K-feldspar	0.63	0.68	0.65	2560	1664	1.664
Plagioclase	-	0.71	0.71	2600	1846	1.846
Biotite	-	0.76	0.76	3090	2348	2.3484
Muscovite	-	0.78	0.76	2820	2143	2.1432
Hornblende	0.75	-	0.75	3230	2423	2.4225
Augite	0.67	0.69	0.68	3400	2312	2.312
Chlorite	0.6	-	0.6	2650	1590	1.59
Titanite	-	-	-	-	-	-
Magnetite	0.6	0.6	0.6	5150	3090	3.09
Ilmenite	0.77	-	0.77	4720	3634	3.6344
Calcite	0.5-0.52	0.5	0.51	2710	1382	1.3821
Apatite	0.8-0.83	0.79	0.81	3190	2584	2.5839
Andradite	-	-	-	-	-	-

Forserum skarn	**Points counted**	**Volume fraction (%)**	**Cv (MJ/m^{3}K)**
Quartz	164	21	0.40
Plagioclase	110	14	0.26
Calcite	241	31	0.42
Andradite	51	6	0.00
Matrix	220.0	28	0.40
Totals	786	100.0	1.48
Forserum diabase	**Points counted**	**Volume fraction (%)**	**Cv (MJ/m^{3}K)**
Plagioclase	515	64	1.19
Ca-clinopyroxene	176	22	0.51
Ilmenite	71	9	0.32
Crack matrix	37	5	0.09
Totals	799	100	2.11
Gillstad	**Points counted**	**Volume fraction (%)**	**Cv (MJ/m^{3}K)**
Quartz	48	6	0.12
Plagioclase	422	55	1.02
Hornblende	80	10	0.25
Ca-clinopyroxene	34	4	0.10
Biotite	101	13	0.31
alteration matrix	69	9	0.21
Magnetite	10	1	0.04
Totals	764	100	2.06
Flivik	**Points counted**	**Volume fraction (%)**	**Cv (MJ/m^{3}K)**
Quartz	231	25	0.48
Plagioclaese	188	24	0.45
K-feldspar	220	34	0.56
Biotite	99	13	0.30
Magnetite	17	2	0.07
Titanite	14	2	0.00
Totals	*769*	*100*	1.86
Fröland	**Points counted**	**Volume fraction (%)**	**Cv (MJ/m^{3}K)**
Quartz	276	36	0.69
Plagioclaese	235	31	0.51
K-feldspar	250	33	0.61
Totals	*761*	100	1.81
Bårarp A	**Points counted**	**Volume fraction (%)**	**Cv (MJ/m^{3}K)**
Quartz	233	29	0.56
Plagioclaese	216	27	0.50
K-feldspar	252	31	0.52
Biotite	72	9	0.21

Hornblende	14	2	0.04
Magnetite	14	2	0.05
Totals	801	100	1.88
Bårarp B	**Points counted**	**Volume fraction (%)**	**Cv (MJ/m^{3}K)**
Quartz	210	26	0.49
Plagioclase	234	29	0.53
K-feldspar	262	32	0.54
Biotite	71	9	0.20
Hornblende	25	3	0.07
Magnetite	12	1	0.05
Totals	814	100	1.88

Appendix 3. The thermal conductivity is calculated by using Equation 6 ($\sum n_{volume\ fraction} * k_{value\ for\ thermal\ conductivity}$) where the volume fraction has to be divided by 100 to get decimal form. The Gillstad matrix is approximated to 50% hornblende, 30% augite, 10% biotite, 5% plagioclase and 5% quartz. The matrix in the skarn is approximated to 50% calcite, 20% plagioclase, 20% quartz and 10% andradite. The fracture matrix consists of 50% adularia (2.05 W/mK), 25% augite and 25% plagioclase. An example could be

$$\lambda_{Fröland} = n_{qz} * k_{qz} + n_{Kfsp} * k_{Kfsp} + n_{ab} * k_{ab}$$
$$= 0.36 * 7.69 + 0.33 * 2.34 + 0.31 * 1.98 = 4.17$$

Mineral phases Flivik	**Points counted**	**Volume fraction (%)**	**Thermal conductivity**	**Parallel equation**
Quartz	193	25	7.68	1.93
Plagioclase(Ab89-An11)	188	24	1.98	0.48
K-feldspar (microcline)	258	34	2.34	0.79
Biotite	99	13	2.02	0.26
Magnetite	17	2	5.10	0.11
Titanite	14	2	2.34	0.04
Totals	*769*	*100*	-	3.61
Mineral phases Fröland	**Points counted**	**Volume fraction (%)**	**Thermal conductivity**	**Parallel equation**
Quartz	276	36	7.68	2.79
Plagioclase (Ab89-An11)	235	31	1.98	0.61
K-feldspar (microcline)	250	33	2.34	0.77
Totals	*761*	100	-	4.17
Mineral phases Bårarp A	**Points counted**	**Volume fraction (%)**	**Thermal conductivity**	**Parallel equation**

Quartz	233	29	7.68	2.24
Plagioclase (Ab89-An11)	216	27	1.98	0.53
K-feldspar (orthoclase)	252	32	2.31	0.73
Biotite	72	9.0	2.02	0.18
Hornblende	14	2	2.80	0.05
Magnetite	14	2	5.10	0.09
Totals	801	100	-	3.82
Mineral phases Bårarp B	**Points counted**	**Volume fraction (%)**	**Thermal conductivity**	**Parallel equation**
Quartz	210	26	7.68	1.98
Plagioclase (Ab89-An11)	234	29	1.98	0.57
K-feldspar (orthoclase)	262	32	2.31	0.74
Biotite	71	9	1.60	0.14
Hornblende	25	3	2.81	0.09
Magnetite	12	2	5.07	0.07
Totals	814	100	-	3.60
Mineral phases Gillstad	**Points counted**	**Volume fraction (%)**	**Thermal conductivity**	**Parallel equation**
Quartz	48	6	7.68	0.48
Plagioclase (Ab_{46}-$An_{54)}$	422	55	1.52	0.84
Hornblende	80	11	2.80	0.29
Augite	34	5	3.82	0.17
Biotite	101	13	2.02	0.27
alteration matrix	69	9.0	3.21	0.29
Magnetite	10	1	5.10	0.07
Totals	764	100	-	2.41
Mineral phases Forserum skarn	**Points counted**	**Volume fraction (%)**	**Thermal conductivity**	**Parallel equation**
Quartz	164	21	7.68	1.60
Plagioclase (Ab_{46}-$An_{54)}$	110	14	1.52	0.21
Calcite	241	31	3.59	1.10
Andradite	51	7	3.09	0.20
Matrix	220	28	4.0	1.13
Totals	786	100	-	4.24
Mineral phases Forserum diabase	**Points counted**	**Volume fraction (%)**	**Thermal conductivity**	**Parallel equation**
Plagioclase (Ab_{46}-$An_{54)}$	513	64	1.52	0.98

Augite	176	22	3.82	0.84
Ilmenite	71	9	2.37	0.21
Fracture matrix (adularia)	37	5	2.36	0.11
Totals	799	100	-	2.08

Appendix 4. 30 grain of quartz (average size 1.55 mm). K-feldspar (average size 2.93 mm) and plagioclase (average size 1.84 mm) was measured in the longest direction in the Flivik specimen. Average grain size of the 90 measurements is 2.11 mm.

Quartz grain size (mm)	**K-feldspar grain size (mm)**	**Plagioclase grain size (mm)**
3	2.5	1.75
1	3.5	1.5
1.75	6	1.25
1.8	3.5	1
1.7	3	2
1	9	4.5
0.3	1.5	2
1.5	2	1.5
3	1	0.8
1.25	7	1.5
1	3	1.5
1	2.5	1.75
2	4	1.25
1.5	1.5	2
0.3	2	1.25
0.4	1.5	1.5
2	4	1.5
1.5	1.75	1.5
2	2	1.5
1.5	5	2
1.5	2	2.5
1.5	3	1.25
3	1.5	1
1	2	1.5
3.5	3.5	3
0.8	1.5	3
1.5	1	2.5
2.5	1.5	1.5
0.5	2	2.5
1.3	3.5	3

Appendix 5. 30 grain of quartz (average size 1.5 mm). K-feldspar (average size 1.38 mm) and plagioclase (average size 1.73 mm) was measured in the longest direction in the Fröland specimen. Average grain size of the 90 measurements is 1.54 mm.

Quartz grain size (mm)	**K-felspar grain size (mm)**	**Plagioclase grain size (mm)**
2	0.75	2
1.75	1.75	2.2
1	2.2	1.2
1.8	2.2	1.5
1.6	1.5	1.8
2.5	1	3
2.5	2	2.2
2.7	2	2
2.2	1	1.5
2	0.75	2
0.3	1.5	1.5
2.5	1.3	2.3
2	0.8	1.5
1	0.8	3.5
1.3	1	2
0.6	0.3	1.5
2	1.75	2
2.5	1	0.7
0.4	4.5	1.3
0.3	0.4	0.8
1	2.5	2
0.7	2	2
1	1.7	1.3
1.5	0.3	1.5
1	1	2
2	1	1
0.3	0.6	1.5
0.5	1.5	0.6
2	0.7	2.5
2	1.5	1

Appendix 6. 30 grain of quartz (average size 0.5 mm). K-feldspar (average size 0.44 mm) and plagioclase (average size 0.61 mm) was measured in the longest direction in the Bårarp B specimen. Average grain size of the 90 measurements is 0.52 mm.

Quartz grain size (mm)	**K-feldspar grain size (mm)**	**Plagioclase grain size (mm)**
0.3	0.4	1
1.1	0.3	0.3
0.4	0.4	0.7
0.6	0.4	0.4
0.5	0.8	0.3
0.15	0.5	0.8
0.2	0.4	0.5
0.2	0.4	0.3
0.8	0.3	0.9
0.5	0.4	0.6
0.6	0.4	0.7
1.2	0.4	1
0.2	3	0.6
0.1	0.2	1
0.2	0.2	0.7
0.7	0.3	1.2
0.3	0.4	0.8
0.1	0.7	0.3
0.7	0.4	0.8
0.3	0.3	0.6
0.5	0.2	0.6
0.2	0.3	0.6
1	0.1	0.3
0.4	0.3	0.8
0.6	0.3	0.3
0.6	0.3	0.3
0.7	0.4	0.4
0.9	0.4	0.5
0.4	0.2	0.4
0.6	0.2	0.8

Appendix 7. 30 grain of plagioclase (average 2.43 mm). augite (0.97 mm) and ilmenite (1.05 mm) was measured in the longest direction in the Forserum diabase specimen. Average grain size of the 90 measurements is 1.49 mm.

Plagioclase grain size (mm)	**Augite grain size (mm)**	**Ilmenite grain size (mm)**
2.2	1.2	2
2.3	1.1	0.5
1.8	0.7	0.6
2.5	1.3	1.2
1.3	1.8	1
1	1.8	0.7
1.7	1	1.1
3	1.1	2.5
2.5	0.5	1.5
2	0.7	1.5
2.3	1	1
3.5	0.5	0.8
3	0.5	2.5
4	0.8	1
0.7	1.5	1
1.5	1.2	2
3.2	0.3	0.8
3	0.6	1
1.5	1.2	0.5
1.5	3	0
2.5	0.5	0.4
4.5	0.8	0.6
1.6	1	1.1
2.2	1	1
2	0.8	0.4
1.5	0.6	1.2
3.5	0.4	0.8
3	0.6	1
3	1	0.9
4.7	0.8	1

Appendix 8. 30 grain of plagioclase (average 1.8 mm). augite (1.01 mm) and ilmenite (0.99 mm) was measured in the longest direction in the Gillstad specimen. Average grain size of the 90 measurements is 1.27 mm.

Plagioclase grain size (mm)	**Augite grain size (mm)**	**Hornblende grain size (mm)**
4.5	0.5	2
2.5	0.3	0.5
0.5	2.5	1
0.5	1	0.9
2	0.5	0.5
1	0.6	0.8
2	3	0.5
1.5	1	0.6
2	1.5	1.1
1.5	0.8	1
3	0.6	0.4
1	1.5	0.9
2	1	1
0.7	0.6	3
2	0.5	1.3
1.5	0.3	1
1.5	0.6	0.9
1.4	0.4	2.5
1	0.5	1.5
3.5	1.1	1
2	1	0.8
3.5	2	0.5
3	1	1
1	0.3	0.3
2.5	0.9	0.7
2	1	1
0.7	0.9	1
0.8	1.3	0.6
2.5	2.1	0.7
0.5	1	0.8

Appendix 9. TPS data of selected parameters and results (graph y-axis represents all thermal property units and x-axis is number of runs) for the Forserum skarn specimen.

Runs	Meas.time (s)	Output power (mW)	Total/Temp.Incr (K)	Th.Conductivity (W/mK)	Th.Diffusivity (mm^2/s)	Vol heat cap (MJ/m^3K)
1	20	700	4.30	3.400244364	1.50518627	2.259018988
2	20	700	4.30	3.397041931	1.503363737	2.259627426
3	20	700	4.32	3.396560119	1.50242475	2.26071896
4	20	700	4.32	3.39728146	1.501954692	2.261906753
5	20	700	4.30	3.397014416	1.501964948	2.26171351
6	20	700	4.30	3.39759306	1.502198422	2.26174719
7	20	700	4.30	3.397158932	1.50357651	2.259385479
8	20	700	4.29	3.397748185	1.502330665	2.261651355
9	20	700	4.27	3.39768461	1.502304788	2.261647994
10	20	700	4.30	3.396587311	1.503233754	2.259520386
11	20	700	4.30	3.39688147	1.502412971	2.260950575
12	20	700	4.27	3.397517673	1.502555786	2.26115909
13	20	700	4.28	3.397165967	1.502884827	2.260430011
14	20	700	4.28	3.397480336	1.501901273	2.26211962
15	20	700	4.30	3.397439514	1.503425971	2.25979834
			stdev	0.00086105	0.000869901	0.001055636
			average	**3.397**	**1.503**	**2.261**
			stdev %	0.025344189	0.057886085	0.046693851

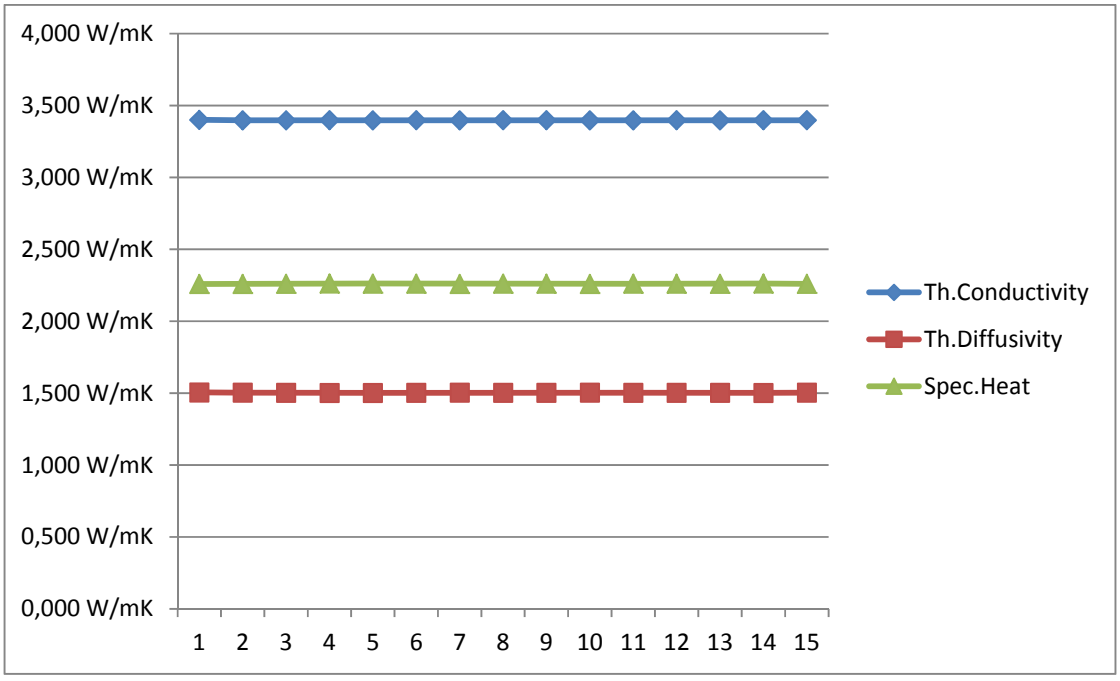

Appendix 10. TPS data of selected parameters and results (graph y-axis represents all thermal property units and x-axis is number of runs) in the Forserum diabase specimen.

Runs	Meas.time (s)	Total/Temp.Incr (K)	Output power (mW)	Th.Conductivity (W/mK)	Th.Diffusivity (mm^2/s)	Vol heat cap (MJ/m^3K)
1	20	4.71	700	2.46204364	1.017829849	2.418914755
2	20	4.72	700	2.461028623	1.015764538	2.422833769
3	20	4.70	700	2.461165592	1.015463914	2.423685922
4	20	4.71	700	2.461216647	1.018941539	2.415464041
5	20	4.72	700	2.461473886	1.016758321	2.420903606
6	20	4.71	700	2.46226433	1.019189101	2.41590528
7	20	4.72	700	2.461207389	1.016270175	2.42180421
8	20	4.71	700	2.461646285	1.018281712	2.41745114
9	20	4.70	700	2.461400508	1.015878192	2.422928781
10	20	4.71	700	2.461185446	1.014978885	2.424863692
11	20	4.71	700	2.462183017	1.015833144	2.42380654
12	20	4.73	700	2.461236116	1.017919506	2.417908393
			stdev	0.000431333	0.001441413	0.003279597
			average	**2.46150429**	**1.016925739**	**2.420539177**
			stdev %	0.017523148	0.14174219	0.135490352

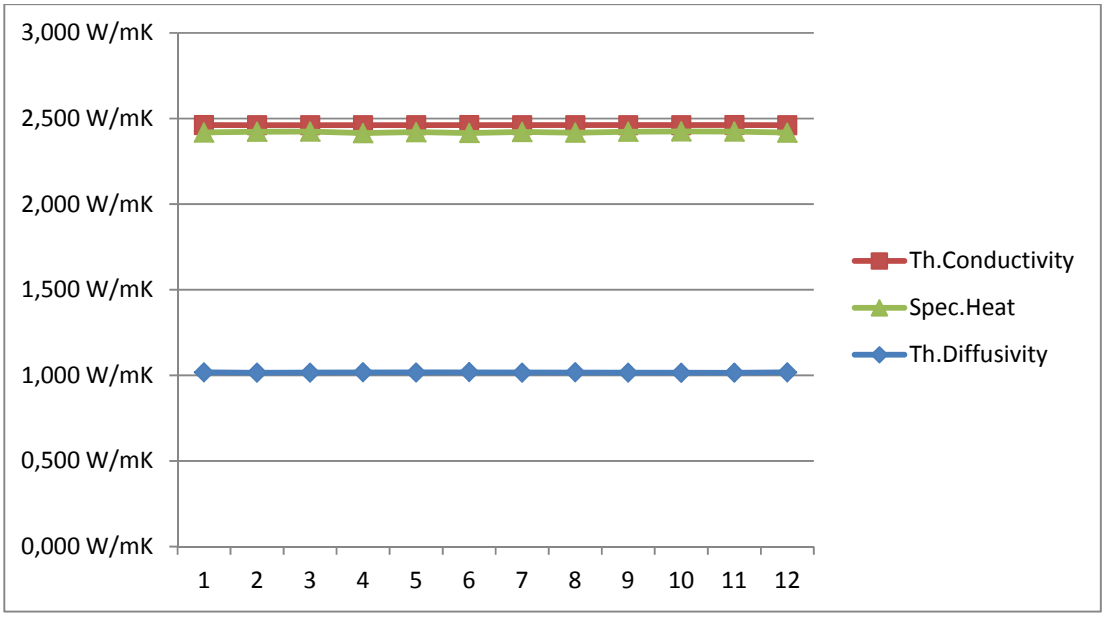

Appendix 11. TPS data of selected parameters and results (graph y-axis represents all thermal property units and x-axis is number of runs) in the Gillstad specimen.

Runs	Meas.time (s)	Total/Temp.Incr (K)	Output power (mW)	Th.Conductivity (W/mK)	Th.Diffusivity (mm^2/s)	Vol heat cap (MJ/m^3K)
1	20	4.70	700	2.562852648	1.136140035	2.25575419
2	20	4.68	700	2.586023647	1.105488741	2.33925824
3	20	4.72	700	2.585873278	1.106442029	2.33710688
4	20	4.71	700	2.576318721	1.117973515	2.30445416
5	20	4.71	700	2.585708976	1.106374462	2.3371011
6	20	4.71	700	2.586446275	1.105815529	2.33894913
7	20	4.71	700	2.5856558	1.108150313	2.33330783
8	20	4.70	700	2.585843325	1.107376569	2.3351075
9	20	4.71	700	2.587490324	1.107309249	2.33673685
10	20	4.70	700	2.58648446	1.103652247	2.34356834
11	20	4.71	700	2.569126883	1.125877926	2.2818876
12	20	4.70	700	2.563923758	1.135816089	2.25734059
13	20	4.71	700	2.585776695	1.110345249	2.32880421
			stdev	0.009230749	0.011614908	0.03202772
			average	**2.58057883**	**1.113597073**	**2.31764436**
			stdev %	0.3577007	1.04300817	1.38190817

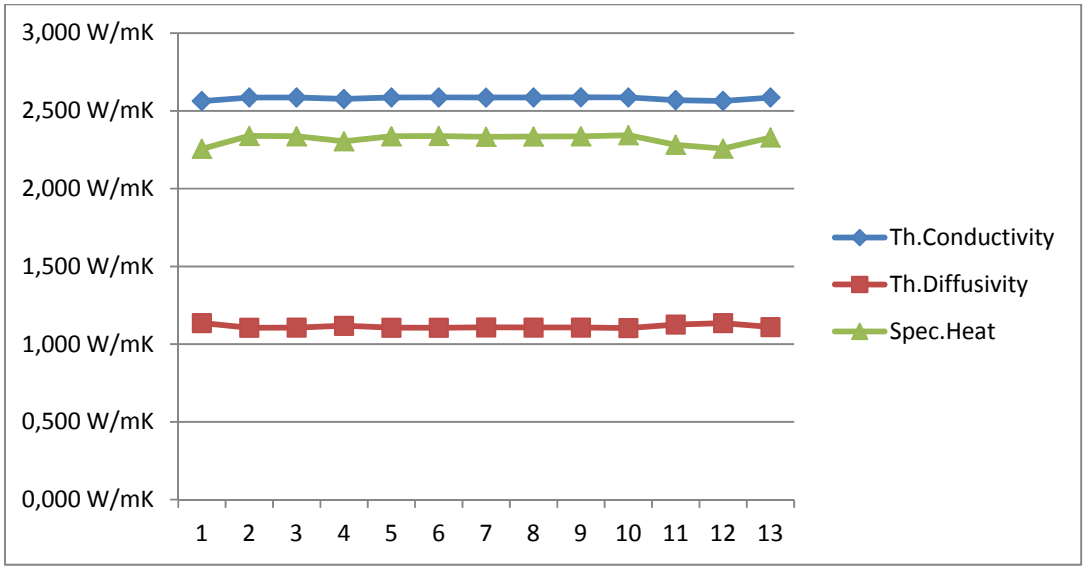

Appendix 12. TPS data of selected parameters and results (graph y-axis represents all thermal property units and x-axis is number of runs) in the Flivik granite specimen.

Runs	Meas.time (s)	Total/Temp.Incr (K)	Output power (mW)	Th.Conductivity (W/mK)	Th.Diffusivity (mm^2/s)	Vol heat cap (MJ/m^3K)
1	20	4.34	700	3.04856972	1.344862818	2.266825791
2	20	4.34	700	3.04566495	1.342433434	2.268764221
3	20	4.31	700	3.04550869	1.339417403	2.273756247
4	20	4.32	700	3.04516541	1.339682291	2.273050429
5	20	4.33	700	3.04422853	1.338840136	2.273780451
6	20	4.30	700	3.04643256	1.337669497	2.277417977
7	20	4.31	700	3.04412708	1.34001029	2.271719182
8	20	4.33	700	3.04391057	1.33747269	2.275867457
9	20	4.33	700	3.04407285	1.340735849	2.270449362
10	20	4.33	700	3.04420515	1.33747269	2.276087711
11	20	4.37	700	3.04355295	1.339036849	2.272941894
12	20	4.37	700	3.0433506	1.336736662	2.27670168
13	20	4.34	700	3.04473748	1.338317488	2.275048715
14	20	4.34	700	3.04413646	1.33812473	2.274927284
15	20	4.34	700	3.0446342	1.334222368	2.281954096
			stdev	0.00133188	0.00248535	0.003692098
			average	**3.04481981**	**1.339002346**	**2.273952833**
			stdev %	0.04374252	0.185612095	0.162364747

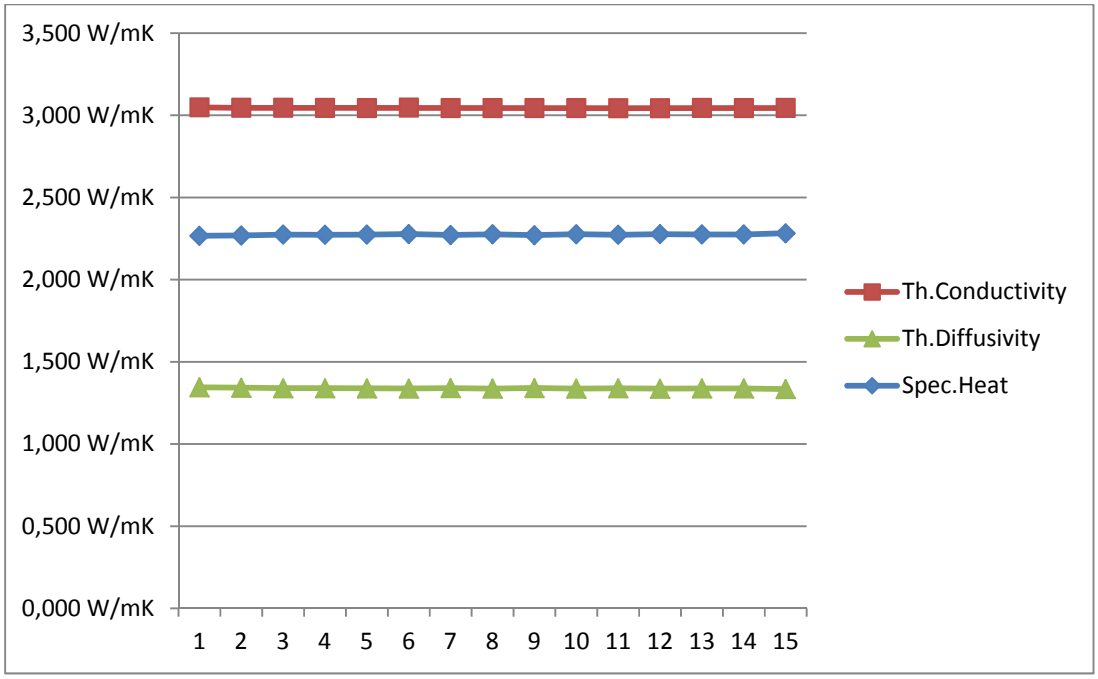

Appendix 13. TPS data of selected parameters and results (graph y-axis represents all thermal property units and x-axis is number of runs) in the Fröland granite specimen.

Runs	Meas.time (s)	Total/Temp.Incr (K)	Output power (mW)	Th.Conductivity (W/mK)	Th.Diffusivity (mm^2/s)	Vol heat cap (MJ/m^3K)
1	20	3.838515504	700	3.815614045	1.654182204	2.30664677
2	20	3.873698674	700	3.816572144	1.636797325	2.33173166
3	20	3.847596786	700	3.818642643	1.631770925	2.34018304
4	20	3.860762653	700	3.816993464	1.634449138	2.3353394
5	20	3.846520613	700	3.818075633	1.633062956	2.33798435
			stdev	0.00120395	0.009207073	0.01363465
			average	**3.817179586**	**1.638052509**	**2.33037704**
			stdev %	0.031540306	0.562074364	0.58508328

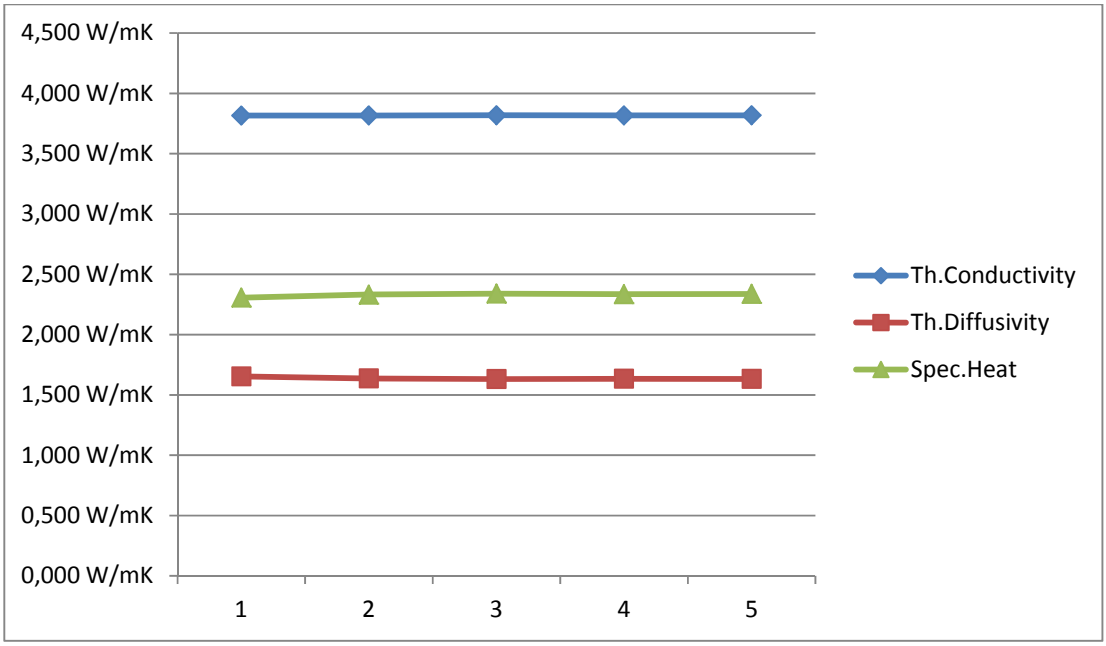

Appendix 14. TPS data of selected parameters and results (graph y-axis represents all thermal property units and x-axis is number of runs) in the Bårarp (A) granitic gneiss.

Runs	Meas.time (s)	Total/Temp.Incr (K)	Output power (mW)	Th.Conductivity (W/mK)	Th.Diffusivity (mm^2/s)	Vol heat cap (MJ/m^3K)
1	20s	5.37	700	2.481273	1.362386	1.821271
2	20s	5.38	700	2.480163	1.361949	1.82104
3	20s	5.40	700	2.474426	1.36718	1.809876
4	20s	5.41	700	2.47406	1.369701	1.806278
5	20s	5.43	700	2.484282	1.353651	1.835246
6	20s	5.39	700	2.48103	1.358331	1.826528
7	20s	5.40	700	2.479783	1.35913	1.824536
8	20s	5.43	700	2.477282	1.363194	1.817263
9	20s	5.42	700	2.478396	1.362371	1.819179
10	20s	5.42	700	2.48228	1.358403	1.827351
11	20s	5.40	700	2.480445	1.359509	1.824515
			stdev	0.005598	0.008758	0.016001
			average	**2.48077**	**1.35922**	**1.82523**
			stdev %	0.225645	0.644365	0.876644

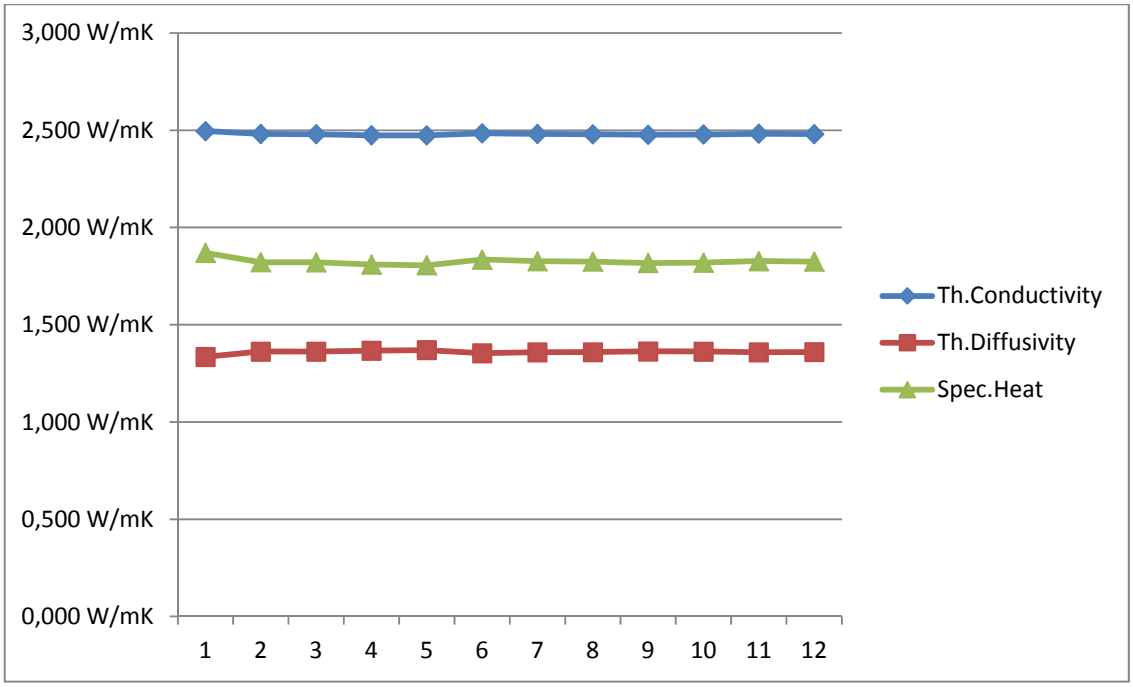

Appendix 15. TPS data of selected parameters and results (graph y-axis represents all thermal property units and x-axis is number of runs) in the Bårarp (B) granitic gneiss.

Runs	Meas.time (s)	Total/Temp.Incr (K)	Output power (mW)	Th.Conductivity (W/mK)	Th.Diffusivity (mm^2/s)	Vol heat cap (MJ/m^3K)
1	20s	5.21	700	2.532808171	1.215627608	2.083539526
2	20s	5.16	700	2.532385103	1.216524166	2.081656224
3	20s	5.18	700	2.531111182	1.216089528	2.081352667
4	20s	5.20	700	2.53845239	1.204018799	2.108316243
5	20s	5.19	700	2.538032427	1.20464691	2.106868332
6	20s	5.20	700	2.529397016	1.216715922	2.07887229
7	20s	5.19	700	2.52993011	1.216901435	2.078993447
8	20s	5.18	700	2.538959679	1.20568482	2.105823709
9	20s	5.22	700	2.528916017	1.218987225	2.074604201
10	20s	5.20	700	2.530822203	1.214063363	2.084588235
11	20s	5.19	700	2.536055949	1.207341812	2.100528552
12	20s	5.22	700	2.530962839	1.212394746	2.08757325
13	20s	5.20	700	2.538270876	1.204521656	2.107285381
14	20s	5.21	700	2.535811918	1.206849792	2.101182711
15	20s	5.21	700	2.534977428	1.207995608	2.098498878
16	20s	5.23	700	2.53782673	1.202103157	2.111155533
17	20s	5.24	700	2.534414907	1.207231052	2.099361927
18	20s	5.20	700	2.529867081	1.214186903	2.0835895
19	20s	5.21	700	2.531411937	1.213379201	2.086249653
20	20s	5.20	700	2.523361432	1.225607541	2.058865784
21	20s	5.20	700	2.528271686	1.218402403	2.075071159
22	20s	5.21	700	2.533007892	1.211030136	2.091614252

23	20s	5.20	700	2.536577564	1.204825705	2.105348145
24	20s	5.24	700	2.531183342	1.212388978	2.087765055
25	20s	5.22	700	2.533695583	1.209595659	2.094663258
26	20s	5.22	700	2.525001721	1.220902576	2.068143496
27	20s	5.19	700	2.531058519	1.211940062	2.088435394
28	20s	5.20	700	2.532659043	1.210839122	2.091656106
29	20s	5.21	700	2.527153047	1.216717013	2.077026145
30	20s	5.19	700	2.528522782	1.21688515	2.07786477
			stdev	0.004029574	0.005770422	0.013141395
			average	**2.532363552**	**1.212146602**	**2.089216461**
			stdev %	0.15912306	0.476049805	0.629010701